Late Quaternary climatic changes revealed by luminescence dating, mineral magnetism and diffuse reflectance spectroscopy of river terrace palaeosols: a new form of geoproxy data for the southern African interior

Lyons, James Richard; Tooth, Stephen; Duller, G. A. T.

Published in:
Quaternary Science Reviews

DOI:
10.1016/j.quascirev.2014.04.021

Publication date:
2014

Citation for published version (APA):
Lyons, J. R., Tooth, S., & Duller, G. A. T. (2014). Late Quaternary climatic changes revealed by luminescence dating, mineral magnetism and diffuse reflectance spectroscopy of river terrace palaeosols: a new form of geoproxy data for the southern African interior. *Quaternary Science Reviews*, *95*, 43-59. https://doi.org/10.1016/j.quascirev.2014.04.021

Quaternary Science Reviews 95 (2014) 43–59

Contents lists available at ScienceDirect

Quaternary Science Reviews

journal homepage: www.elsevier.com/locate/quascirev

Late Quaternary climatic changes revealed by luminescence dating, mineral magnetism and diffuse reflectance spectroscopy of river terrace palaeosols: a new form of geoproxy data for the southern African interior

Richard Lyons [a,b,*], Stephen Tooth [a,b], Geoff A.T. Duller [a]

[a] Department of Geography and Earth Sciences, Aberystwyth University, Ceredigion, SY23 3DB, Aberystwyth, UK
[b] School of Geosciences, University of the Witwatersrand, Johannesburg, Private Bag 3, South Africa

ARTICLE INFO

Article history:
Received 27 December 2013
Received in revised form
3 April 2014
Accepted 18 April 2014
Available online 20 May 2014

Keywords:
Erfkroon
Southern Africa
Palaeosol
OSL
Quaternary
Mineral magnetism

ABSTRACT

The nature, spatial patterns and forcing mechanisms of Quaternary climatic changes across southern Africa remain unresolved and contentious, principally due to the scarcity of continuous and robustly-dated proxy records. We present what we interpret to be a broadly continuous record of late Quaternary climatic change based on optically stimulated luminescence (OSL) dating, and mineral magnetic and diffuse reflectance spectroscopy (DRS) analyses of stacked palaeosols within an overbank alluvial succession along the Modder River, central South Africa. The OSL ages indicate that alluvial sedimentation occurred at a fairly steady rate, averaging ~0.15 mm/yr from at least 44 ka until ~0.83 ka. This suggests that the palaeosols are accretionary, having formed contemporaneously with sedimentation. Climate is identified as the key soil-forming factor controlling the intensity of pedogenesis and is reflected in the changing concentration of pedogenic ferrimagnetic minerals (magnetite/maghemite) of single domain and superparamagnetic dimensions, and by variations in the amount of hematite compared to goethite. These data indicate that the climate was generally dry (rainfall ~200–400 mm/yr) from ~46 to 32 ka, except for a brief peak in humidity at ~42 ka. There was then a period of greater humidity (rainfall ~400–600 mm/yr) from ~32 to 28 ka, possibly reflecting enhanced moisture supply from the Atlantic Ocean associated with the equatorward migration and intensification of westerly storm tracks. Although the precise mechanism remains unresolved, this climatic change may have been linked to an obliquity minimum at ~29 ka. After ~28 ka, the climate became progressively cooler and drier, especially between ~18 and 15.5 ka when rainfall was as low as ~100–200 mm/yr. Temperatures and rainfall then increased from ~15.5 ka onwards, with the latter possibly linked to rising sea-surface temperatures in the SW Indian Ocean and enhanced moisture supply from easterly circulation. At ~0.83 ka, a time corresponding with part of the Medieval Climatic Anomaly (MCA, ~900–1300 AD), rainfall reached ~600–700 mm/yr and was higher than at present (~400–500 mm/yr). Fluvial landforms have previously been overlooked as a source of palaeoenvironmental information in southern Africa, but this study clearly demonstrates the potential to extract robust palaeoenvironmental data from alluvial-palaeosol successions in the arid to semi-arid interior where other forms of proxy record are scarce.

1. Introduction

The dominantly arid to semi-arid climate of interior southern Africa generally precludes the production and preservation of organic-based proxies that traditionally are used to date and reconstruct Quaternary environmental changes. The resulting scarcity of long, continuous and robustly-dated palaeoenvironmental datasets has hindered progress towards resolving the nature, spatial patterns and forcing mechanisms of Quaternary climatic changes (Chase and Meadows, 2007). Given the lack of organic-based proxies, southern African palaeoenvironmental data is largely derived from spatially pervasive geomorphological landforms such as sand dunes and palaeolake shorelines (Thomas

* Corresponding author. School of Geosciences, University of the Witwatersrand, Johannesburg, Private Bag 3, South Africa. Tel.: +27 (0)11 717 6542.
E-mail addresses: richardlyons810@msn.com, richard.lyons@wits.ac.za (R. Lyons).

http://dx.doi.org/10.1016/j.quascirev.2014.04.021

and Burrough, 2012). Palaeoenvironmental information can be extracted from these so-called 'geoproxies' because their sedimentology, morphology and spatial distribution may have been controlled by past environmental (e.g. climatic) changes (Thomas and Burrough, 2012, in press; Thomas, 2013). Although our ability to robustly date dune and palaeolake geoproxies using optically stimulated luminescence (OSL) techniques has greatly advanced (Duller, 2004; Tooth, 2012), little consensus has emerged as to the interpretation and palaeoenvironmental significance of the resulting datasets (e.g. Burrough et al., 2009; Chase, 2009; Thomas and Burrough, in press). Moreover, these geoproxy datasets often conflict with other proxy datasets, which has resulted in their exclusion from some regional syntheses of late Quaternary environmental and climatic change (Chase and Meadows, 2007).

Fluvial sedimentary landforms (e.g. alluvial river terraces) offer an additional source of geoproxy data for southern Africa (e.g. Shaw et al., 1992; Verster and van Rooyen, 1999), but are yet to be investigated in any detail. This is probably due to the fact that alluvial successions are often discontinuous and robust chronologies have traditionally been difficult to establish. Nevertheless, despite some ambiguities in interpretation, studies in other dryland locations have demonstrated the potential of fluvial systems to record palaeoenvironmental changes (e.g. Nanson and Tooth, 1999; Tooth, 2007; Reid, 2009). There is considerable opportunity to address this research deficiency in interior South Africa, particularly where extensive river channel and donga (gully) incision (Tooth et al., 2004; Keen-Zebert et al., 2013; Lyons et al., 2013) has resulted in widespread alluvial exposures. In many cases, alluvial exposures reveal detailed stratigraphy, palaeosols and archaeological remains that may be of palaeoenvironmental significance (e.g. Butzer, 1971; Verster and van Rooyen, 1999; Churchill et al., 2000; Tooth et al., 2013). To explore this opportunity, this paper focuses on the site of Erfkroon, situated along the middle reaches of the Modder River, western Free State, central South Africa (Fig. 1). Here, deep river channel and donga incision has exposed an ~15 m thick alluvial succession, with the uppermost ~8 m hosting four stacked palaeosols (Tooth et al., 2013). These palaeosols contain rich and diverse fossil faunal (e.g. extinct and extant wetland, aquatic and grassland species), as well as archaeological assemblages, including lithics associated with the African Middle (~240–25 ka) and Later (~25 ka to historic times) Stone Ages (Churchill et al., 2000). Although Tooth et al. (2013) previously used infrared stimulated luminescence and OSL dating techniques to establish the late Quaternary antiquity of the overbank succession (last ~42 ka), the chronology was of insufficient resolution for detailed investigations of the palaeosols. If the palaeosols contain palaeoclimatic signatures, however, this provides an opportunity to elucidate the nature of palaeoclimatic changes in a region of interior southern Africa notably devoid of robust palaeoenvironmental datasets. In particular, given its location in central South Africa, Erfkroon may help to clarify the dynamic interplay between westerly (Atlantic Ocean) and easterly (Indian Ocean) atmospheric circulation systems during the Quaternary, both of which are key determinants of moisture supply to the interior of southern Africa (Chase and Meadows, 2007; Gasse et al., 2008).

In a range of environmental settings, mineral magnetic measurements of palaeosols have helped to reconstruct palaeoclimatic changes. This is best exemplified by studies of loess-palaeosol

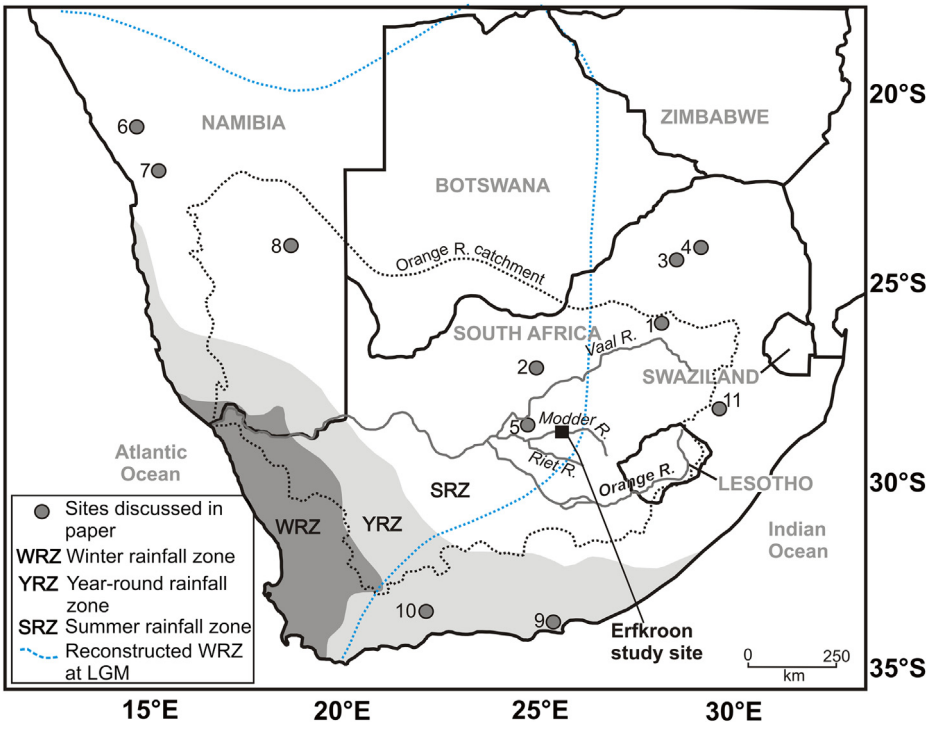

Fig. 1. Map showing the location of the Modder River within the Orange River catchment (black dotted line) and the location of the Erfkroon study site (28°52′09.2″S, 25°35′40.7″E) along the middle reaches of the Modder River. The present extent of the winter rainfall zone (>66% of mean annual rainfall falls between April–September), summer rainfall zone (>66% of mean annual rainfall falls between October–March) and year-round rainfall zone is shown (Chase and Meadows, 2007). The blue dashed line indicates the reconstructed position of the winter rainfall zone during the Last Glacial Maximum (LGM), as proposed by Chase and Meadows (2007). Sites referred to in the text are also shown: 1) Lake Tswaing (Partridge et al., 1997; Schmidt et al., 2014); 2) Equus Cave (Johnson et al., 1997); 3) Wonderkrater (Scott et al., 2003; Truc et al., 2013); 4) Cold Air Cave (Lee-Thorp et al., 2001; Holmgren et al., 2003); 5) Alexandersfontein (Butzer et al., 1973; Butzer, 1984); 6) and 7) Austerlitz and Spitzkoppe hyrax middens, respectively (Chase et al., 2009, 2010); 8) Stampriet aquifer (Stute and Talma, 1998); 9) Uitenhage aquifer (Stute and Talma, 1998); 10) Boomplaas Cave (Thackeray, 1990); and 11) Braamhoek wetland (Norström et al., 2009). (For interpretation of the references to colour in this figure legend, the reader is referred to the web version of this article.)

sequences on the Chinese Loess Plateau, which have contributed to reconstruction of changes in the intensity of the East Asian Monsoon (e.g. Zhou et al., 1990; Maher and Thompson, 1995; Hao et al., 2008). By characterising the response of palaeosol samples to laboratory applied magnetic fields, estimations can be made of the composition, concentration and grain size distribution of magnetic minerals, especially iron oxides that include magnetite (Fe_3O_4), maghemite (γFe_2O_3), hematite (αFe_2O_3), and goethite (αFeOOH) (Liu et al., 2012). This information can then be used to reconstruct changes in palaeoenvironmental conditions, because the nature of soil magnetic iron oxide assemblages is often closely linked with environmental factors, including climate (e.g. Maher, 1998; Maher et al., 2003a; Lyons et al., 2010, 2012). For example, numerous investigators have demonstrated a close link between the magnetic enhancement of surface soil horizons by the pedogenic formation of ultrafine ($<\sim$100 nm) ferrimagnetic minerals (magnetite/maghemite) and annual rainfall (e.g. Maher et al., 2003a; Balsam et al., 2011). Diffuse reflectance spectroscopy (DRS) has also been used to characterise iron oxides in palaeosols, especially hematite (Hm) and goethite (Gt), which play an important role in controlling soil colour (Torrent and Barron, 2002). Given that hematite and goethite are often associated with contrasting climatic conditions (Schwertmann and Taylor, 1989), Hm/(Hm + Gt) ratios have been shown to provide insight into changing temperature and moisture regimes (e.g. Ji et al., 2004; Hao et al., 2009). Combined with the establishment of OSL chronologies, investigation of palaeosols in alluvial exposures across interior South Africa thus may enable a new suite of geoproxy datasets to be generated. Developing novel approaches to extracting palaeoclimatic information from landforms is crucial for enhancing the spatial coverage of palaeo-datasets across southern Africa more generally, and ultimately for developing a clearer picture of the nature, spatial patterns and forcing mechanisms of Quaternary climatic changes.

Against this backdrop, the paper has four main aims: 1) use OSL dating to establish a higher resolution chronology for the overbank part of the alluvial succession at Erfkroon; 2) determine the mineral magnetic and DRS properties of the host palaeosols and establish the palaeoclimatic implications of these results; 3) compare the palaeoclimatic changes recorded in the palaeosols with marine core and other terrestrial southern African proxy records in order to understand the drivers of past climatic change; and 4) assess the potential importance of fluvial geoproxies more generally as a source of palaeoenvironmental data in the dryland interior of southern Africa.

2. Site description and stratigraphy

The Modder River catchment (17 360 km^2) (Barker, 2011) forms part of the larger Orange River catchment and is situated on South Africa's high elevation interior plateau (Fig. 1). Rivers in the region typically have beds that are positioned on, or close to, bedrock that includes late Archaean basement and Palaeozoic to Mesozoic igneous and sedimentary lithologies. These lithologies have variable resistance to fluvial erosion, which has led to the formation of stepped river profiles. Increased gradients occur where channels flow across resistant lithologies (e.g. dolerite sills and dykes of the Karoo Supergroup), and more subdued gradients occur over less resistant sedimentary rocks (e.g. tillites and marine shales associated with the Dwyka and Ecca groups of the Karoo Supergroup). In lower gradient reaches, channels are commonly deeply incised (up to $\sim$20 m) into alluvium and bedrock, and dongas have formed extensively in adjacent floodplain or terrace deposits (Tooth et al., 2013). Distal from the channels, floodplains and dongas, the relief is typically subdued and incorporates ancient, exhumed glacial surfaces or denudational plains characterised by pans (Holmes and Barker, 2006). The subdued relief is interrupted by ridges formed by exhumed dolerite dykes, and mesas and escarpments typically capped by dolerite sills. Away from the floodplains, soils in the region are commonly defined as duplex soils and are characterised by their red, sandy apedal A horizons and aeolian component (Holmes and Barker, 2006). Vegetation in the western Free State reflects a transition from the dry Highveld grassland to Kalahari Hardveld Bushveld vegetation types (Kruger, 2004; Mucina and Rutherford, 2006).

At the Erfkroon study site (1210 masl) (Fig. 1), the geology mainly comprises erodible mudrocks and minor siltstone of the Ecca Group (Karoo Supergroup), but resistant dolerite sills and dykes crop out locally. Erfkroon is situated within southern Africa's summer rainfall zone (SRZ, see Fig. 1) (Chase and Meadows, 2007). Present-day mean annual rainfall at Erfkroon is $\sim$400–500 mm, with moisture predominantly supplied from the SW Indian Ocean by the tropical easterlies (Goddard and Graham, 1999). Annual evaporation (1000–1500 mm) is at least double mean annual rainfall, leading to strongly moisture deficient conditions. At present, the river channel at Erfkroon has incised through an $\sim$15 m thick alluvial succession and $\sim$5 m into shale bedrock. Dongas have eroded headward from the steepened channel banks, creating extensive badland-type terrain (Fig. 2A). The stratigraphy and sedimentary architecture of the alluvial succession at Erfkroon has been reported in detail by Tooth et al. (2013) and is summarised in Fig. 2B. The succession consists of three lower coarse-grained channel units, which represent bedload that was deposited by a relatively high energy, dominantly laterally-migrating channel of the palaeo-Modder River, and a finer-grained overbank succession largely deposited by a lower energy, vertically aggrading channel. This overbank succession hosts four stacked palaeosols (from oldest to youngest: lower grey, red, upper grey and brown) (Fig. 2B). Further details of the overbank succession are presented in Table 1. Proximal to the modern channel, relatively homogenous units of predominantly silty sand cross-cut the entire succession, and on stratigraphic grounds are the youngest units, having formed following a phase of deep channel incision and donga formation (Tooth et al., 2013). The modern surface adjacent to the dongas is covered by an $\sim$0.25 m thick, little weathered silty sand cap (Table 1), which was probably mostly deposited at the same time as the silty sand and palaeodonga fills.

3. Methods

Investigation focused on the overbank succession at Erfkroon, because the preliminary work of Tooth et al. (2013) suggested the potential for deriving a rich palaeoenvironmental record from the palaeosols. In this study, we coupled OSL analyses with mineral magnetic and DRS measurements, as detailed below.

3.1. Field sampling

Sampling was conducted at an $\sim$6–7 m thick, near-vertical exposure of the overbank succession on the sidewall of a donga (Fig. 2B). A total of nine samples were collected for dating using OSL. Sampling targeted the upper and lower portions of each palaeosol, but leaving at least 20 cm from the contacts with underlying or overlying palaeosols. An additional sample was taken from the centre of the red palaeosol, which is the thickest unit. The basal portions of the lower grey palaeosol were not exposed and therefore were not sampled. Samples were retrieved by hammering light-tight steel tubes horizontally into the exposure. The tubes were then extruded without exposing the sediment to light and subsequently wrapped in light-tight black plastic. For

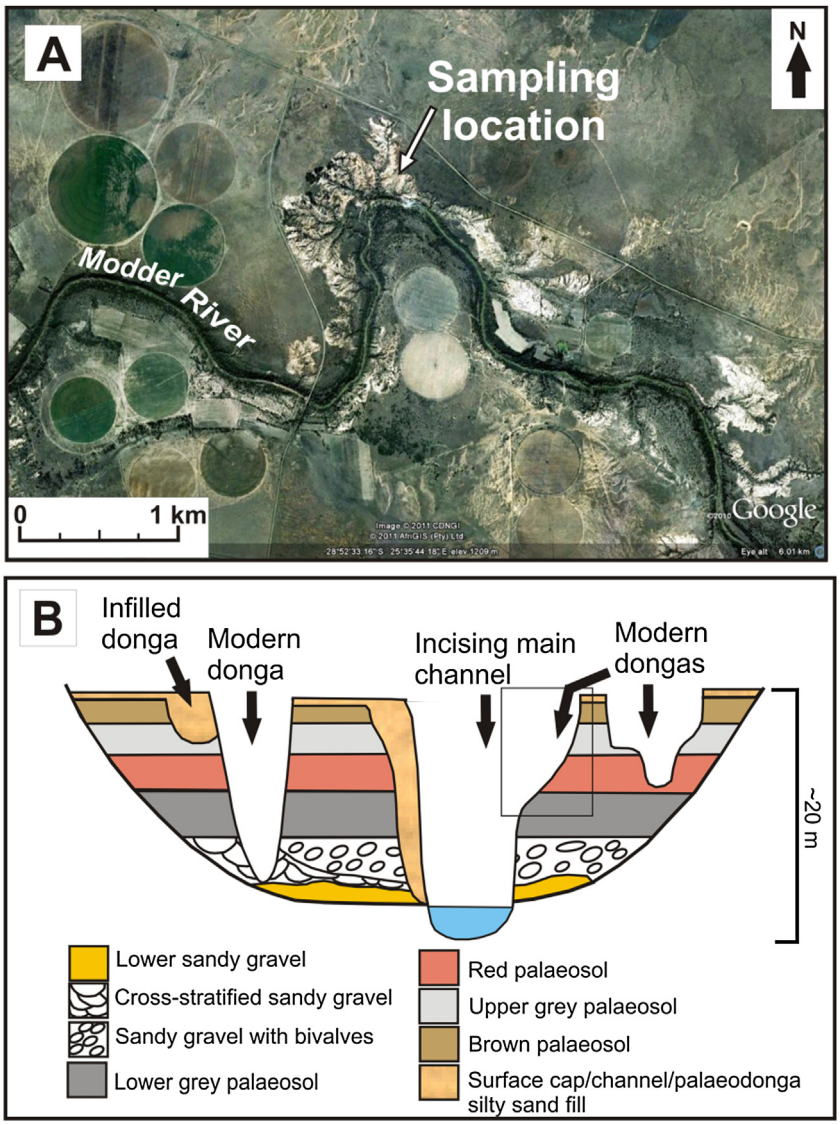

Fig. 2. A) Aerial photograph of the Erfkroon study site. Note the badland-type terrain that is adjacent to parts of the river channel (source: Google Earth). B) Schematic diagram summarising the present stratigraphy at Erfkroon (see Tooth et al., 2013 for further details). The box represents the portion of the overbank succession shown in Fig. 4.

mineral magnetic and DRS measurements, samples were collected at 0.2 m intervals from 0 to 6.6 m depth at the same location.

3.2. OSL analyses

Sample preparation for OSL analyses was carried out under subdued red-light conditions. Samples were subject to a series of acid, dry sieving, and density separation treatments to isolate quartz in the 180–212 μm range, including: i) 10% HCl to dissolve carbonates; ii) 20% H_2O_2 to dissolve organic matter; iii) dry sieving to extract the 180–212 μm grain size fraction; iv) density separation of this fraction to isolate quartz from other minerals using sodium polytungstate solutions; and v) treatment of the quartz bearing fraction with 40% HF acid for 45 min to dissolve any remaining feldspar grains and to remove the outer 10 μm rind of the quartz grains, which is affected by alpha irradiation. Etched quartz grains were then mounted onto the inner 2 mm of 1 cm aluminum discs using Silkospray. On average, each disc contained ~30 grains and are equivalent to 'small' aliquots (Duller, 2008). Single-grain measurements (see below) were performed using a 9.7 mm diameter aluminium disc with one hundred 300 μm deep and 300 μm wide holes. The size of the holes means that only one grain of 180–212 μm quartz is retained in each hole.

OSL samples were analysed using the single aliquot regenerative dose protocol (Murray and Wintle, 2000) on a Risø Automated TL/OSL-DA-15 OSL system, equipped with optical stimulation from blue light emitting diodes. Fig. 3A shows a typical OSL decay curve, and illustrates the rapid initial decay of the OSL signal, indicative of a signal dominated by the fast component. Based on preheat plateau, dose-recovery and thermal transfer tests between 180 and 300 °C, a preheat temperature of 260 °C for 10 s was used for all samples. An example of a SAR dose response curve for an aliquot is shown in Fig. 3B. Small aliquots were used to determine OSL ages, but single-grain measurements were used for MDER10 due to the limited availability of quartz in the 180–212 μm range. Single-grain measurements were also performed for four samples to test for averaging effects that may arise where a large number of grains with contrasting residual doses (a scenario common in fluvially deposited sediments) contribute to the luminescence signal (Duller, 2008). For fluvial samples, this can act to obscure partial bleaching

Table 1
Details and depths of the silty sand cap and palaeosols in the overbank succession at Erfkroon. Textural classification and terminology follows Gale and Hoare (1992).

Unit	Depth (m)	Details
Silty sand cap	0–0.25	Brown (7.5YR 5/4) silty, fine to medium sand, weak fine subangular blocky structure, fine roots, localised charcoal, abrupt smooth lower contact.
Brown palaeosol	0.25–1.3	Brown (7.5YR 5/4) sandy mud to muddy sand, moderate medium subangular blocky structure, minor calcium carbonate rhizocretions and flecks, manganese oxide flecks on ped faces, gradational contact with underlying grey palaeosol.
Upper grey palaeosol	1.3–3.1	Light yellowish brown (10YR 6/4) to strong brown (7.5YR 5/6) sandy mud to mud, weak to moderate medium subangular blocky structure, dispersed calcium carbonate flecks, small nodules and minor rhizocretions (<0.5 cm), disseminated gypsum crystals up to ~1 cm in size particularly in lower portions of the palaeosol, gradational contact with underlying red palaeosol.
Red palaeosol	3.1–5.0	Yellowish red (5YR 5/6) to strong brown (7.5YR 5/6) sandy mud to muddy sand, weak to moderate angular blocky structure, flecks and small (<0.5 cm) calcium carbonate nodules commonplace, manganese oxide staining on ped faces, disseminated gypsum crystals up to ~1 cm in size present locally, thin (<5 cm) discontinuous layer of gypsum crystals up to several cm in size found locally at upper boundary, gradational contact with underlying lower grey palaeosol.
Lower grey palaeosol	5.0–7.0+	Yellowish brown (10YR 5/6) to strong brown (7.5YR 5/6) sandy mud to muddy sand, medium angular blocky structure, small (<1 cm) nodules and flecks of calcium carbonate throughout, manganese oxide staining on ped faces, disseminated gypsum crystals up to ~1 cm in size present locally, lower boundary not observed.

and lead to age overestimation, though Jain et al. (2004) suggest that this is rarely a problem for fluvial samples older than ~1 ka. For the samples measured here, the single-grain measurements indicated that no more than 3% of grains contributed to the luminescence signal and thus small aliquots are likely to be dominated by the OSL signal from one or two grains. This inference was confirmed by the observation that small aliquot and single-grain equivalent dose (D_e) distributions are closely comparable.

For small aliquot measurements, at least 48 aliquots were run for each sample and age determination was based on a minimum of 30 accepted aliquots. Aliquots were rejected on the basis of: i) insufficient count rates; ii) a recycling ratio more than 10% from unity (20% for single-grains); iii) detection of feldspar contamination (IR-OSL depletion ratio more than 10% and 20% from unity for small aliquots and single-grains, respectively) (Duller, 2003); iv) inability to fit an exponential or exponential plus linear function to the growth curve; and v) the luminescence signal not being dominated by the fast component.

For single-grain measurements (e.g. Jacobs and Roberts, 2007; Duller, 2008), individual grains were stimulated with a Nd:YVO_4 laser (beam diameter ~0.02 mm when it strikes a grain) with an emission wavelength of 532 nm and a stimulation power of 10 mW. Overall, samples displayed rapidly bleachable OSL signals dominated by the fast component, low thermal transfer, good recycling and little evidence of feldspar contamination (only 3% of aliquots failed the IR-OSL depletion ratio test).

The uppermost, and also youngest, two samples from the succession (MDER10 and 11) display dose distributions indicative of partial bleaching (overdispersion (σ_{OD}) values of 108 and 46%, respectively), characterised by a sharp lower-leading edge of D_e values and a scatter of higher D_e values above (Jain et al., 2004). This is illustrated for sample MDER10 in Fig. 3C. To generate a single D_e value for age calculation from the D_e distributions of these samples, the Minimum Age Model (MAM) was used (Galbraith et al., 1999). This model is commonly used to select only the most fully bleached component of samples displaying partial bleaching. In contrast, single D_e values for all other (older) samples were calculated using the Central Age Model (CAM), which is used for samples with a single population of D_e values. These older samples have σ_{OD} values between 17 and 30% and do not show asymmetry in their dose distributions (Fig. 3D). This form of distribution contrasts to the asymmetric distributions typically associated with partially bleached fluvial samples (Fig. 3C) (e.g. Rodnight et al., 2006). Previous studies (e.g. Alexanderson and Murray, 2007; Rowan et al., 2012) have also taken a lack of asymmetry in their dose distributions to indicate that their samples were not affected by incomplete bleaching. Moreover, the impact of any partial bleaching that may have been present at deposition becomes less significant for older (>~1 ka) samples (Jain et al., 2004).

Chemical analyses of the samples collected for OSL measurement were carried out at Royal Holloway, University of London, using inductively coupled plasma-mass spectrometry (ICP-MS) and inductively coupled plasma-atomic emission spectrometry (ICP-AES) to determine K, and U and Th concentrations, respectively. These concentrations were converted to environmental dose rates (Gy/ka) using the conversion factors of Adamiec and Aitken (1998). The contribution of cosmic rays to the dose rate was determined according to the techniques of Prescott and Hutton (1994).

3.3. Mineral magnetic measurements

To investigate the mineral magnetic properties of the palaeosols and changes in the intensity of pedogenesis, samples were packed into 10 cc plastic (diamagnetic) pots and subjected to the following sequence of routine magnetic measurements (Walden et al., 1999): i) low frequency (0.47 kHz) magnetic susceptibility (χ_{LF}); ii) high frequency (4.7 kHz) magnetic susceptibility (χ_{HF}); iii) susceptibility of anhysteretic remanent magnetisation (χ_{ARM}); iv) saturation isothermal remanent magnetisation (SIRM) at 1 T; and v) isothermal remanent magnetisation at successively increasing reverse fields of −20, −40, −100 and −300 mT.

Low (χ_{LF}) and high (χ_{HF}) frequency magnetic susceptibility measurements were carried out using a Bartington Instruments MS2B Meter and dual frequency well sensor to assess bulk magnetic mineral concentrations (Dearing, 1994). The difference between the measurements at the two frequencies was then used to calculate the frequency-dependent susceptibility ($\chi_{FD} = \chi_{LF} - \chi_{HF}$), which can also be expressed as a percentage of the low frequency susceptibility (χ_{LF}) value ($\chi_{FD}\% = ((\chi_{LF} - \chi_{HF})/\chi_{LF}) \times 100$). The loss of susceptibility between the two frequencies reflects the response of grains close to the border (around 25 nm in diameter) between Single Domain (SD, ~25–100 nm) and superparamagnetic (SP, <~25 nm) grains (Worm, 1998). This boundary separates those grains that can retain a stable remanence at room temperature from the finest grains, the orientations of which are thermally randomized. The χ_{FD} values often provide an indication of the concentration of fine ferrimagnetic grains (magnetite/maghemite) formed during weathering and pedogenesis (e.g. see Hao et al., 2008). Anhysteretic remanences were grown using a DTECH demagnetizer in a peak alternating field of 100 mT and with a steady DC biasing field of 0.1 mT, and expressed as the susceptibility of ARM (χ_{ARM}) by dividing the ARM by the DC biasing field. This measurement is particularly sensitive to the concentration of ferrimagnetic minerals in the SD size range. Isothermal remanences

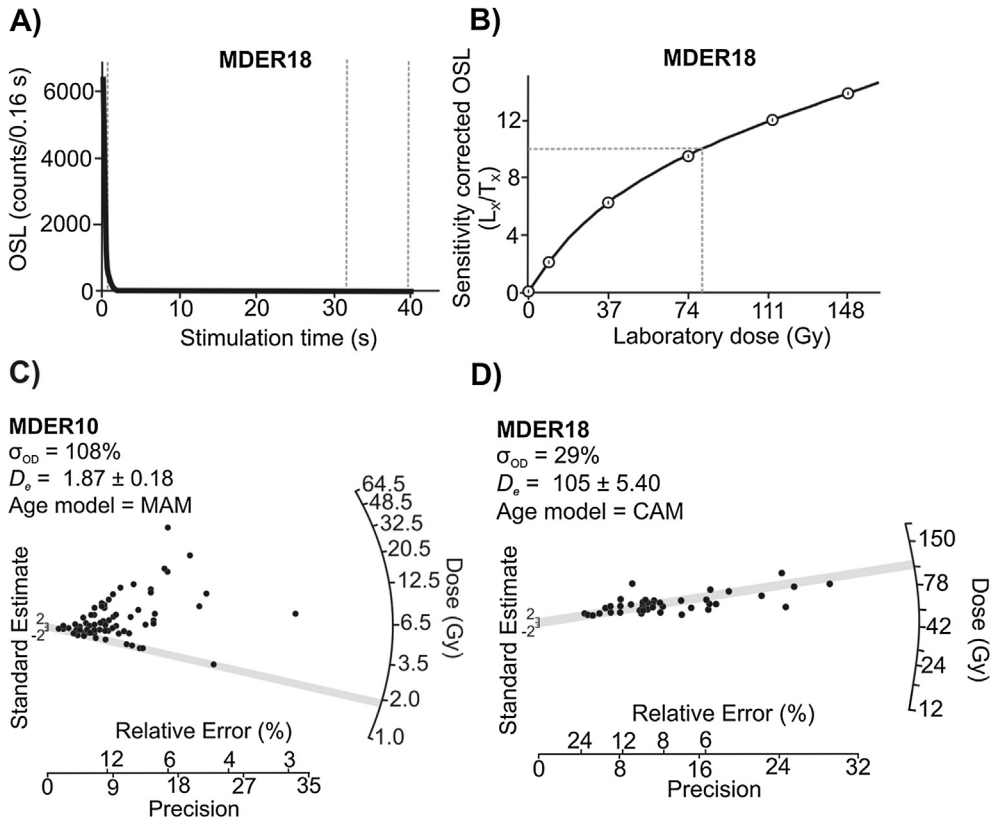

Fig. 3. Plots showing representative OSL results, including: A) the natural signal against stimulation time for sample MDER18, which highlights that the signal is dominated by the fast component (vertical grey dashed lines denote the background signal); B) dose response curve for an individual aliquot of sample MDER18, which highlights that D_e values (grey dashed line) are not near saturation. Lx/Tx is the OSL signal from the aliquot (Lx) normalised by the signal from the fixed test dose (Tx); C) and D) radial plots displaying typical D_e distributions (solid circles) for samples MDER10 (single grains) and MDER18 (small aliquots). The grey bar denotes the dose value used for age calculation, using either the Minimum Age Model (MAM) or Central Age Model (CAM).

were grown using a MMPM5 Pulse Magnetizer with the main objective of assessing the concentration and relative proportions of low (ferrimagnetic) and high (antiferromagnetic) coercivity magnetic phases. All remanences were measured using a Molspin spinner magnetometer with a noise level of $\sim 0.1 \times 10^{-8}$ Am^2. From these measurements a range of additional parameters was subsequently calculated to provide further information on magnetic grain size and mineralogy. These include the quotients χ_{ARM}/SIRM and χ_{ARM}/χ_{LF}, which have often been interpreted as roughly proportional to the relative importance of SD grains, but their interpretation depends on whether the assemblage of ferrimagnetic minerals under consideration is predominantly greater or less than SD (e.g. Oldfield and Yu, 1994; Oldfield and Crowther, 2007). In this paper, we focus particularly on those parameters that are sensitive to secondary magnetic enhancement by fine ferrimagnetic grains, and which thus indicate changes in the intensity of weathering and pedogenesis. Table 2 summarises the interpretation of the magnetic parameters used, and further details can be found in several earlier publications (e.g. Walden et al., 1999; Maher, 2011).

3.4. DRS measurements

To determine the ratio between hematite and goethite concentration in the Erfkroon samples, we used diffuse reflectance UV–Vis spectroscopy (DRS) (Torrent and Barron, 2002; Torrent et al., 2007). The samples were dried, powdered to <10 μm and pressed to pellets using a 15 ton hydraulic press. A Thermo Evolution 300 UV–Vis Spectrophotometer equipped with a Praying Mantis Diffuse Reflectance Accessory (Thermo Scientific) was then used to record the diffuse reflectance spectra from 190 to 1100 nm at 0.5 nm steps at a scan rate of 30 nm/min. The Praying Mantis uses all-aluminium coated optics, rather than traditional integrating spheres, allowing an extended optical range. For each sample, the spectrum of reflectance (R) was transformed using Kubelka–Munk (K–M) remission function [$F(R) = (1 - R)^2/2R$)]. To characterise the iron oxides present, we used the 2nd derivative of $F(R)$ by applying a cubic Savitzky-Golay polynomial fitting to reduce background noise and produce well-resolved absorption bands at the wavelength bands ~425 nm and ~535 nm, which are reflective of goethite and hematite concentrations, respectively (Scheinost et al., 1998). As proposed by Scheinost et al. (1998), we have used the amplitude difference between the ~415 nm minimum and the ~445 nm maximum for goethite (A^{Gt}), and the ~535 nm minimum and ~580 nm maximum for hematite (A^{Hm}). Liu et al. (2011) note that quantitative determinations of hematite and goethite using DRS are unlikely to be reliable where the forms, degree of aluminium substitution and grain sizes are likely to be variable. Therefore we have limited use of the DRS data only to estimation of the ratio of hematite (Hm) to goethite (Gt), which is calculated as Hm/(Hm + Gt).

4. Results

4.1. OSL chronology

Table 3 presents the OSL analytical data and ages, and Fig. 4 shows the OSL ages in the context of the overbank succession. The ages increase with depth and are therefore internally

Table 2
The magnetic and DRS parameters used in this study, their units and interpretation.

Magnetic or DRS parameter	Units	Interpretation
Low frequency magnetic susceptibility (χ_{LF})	10^{-8} m^3/kg	Bulk ferrimagnetic mineral content (especially magnetite/maghemite), but more sensitive to superparamagnetic (<~25 nm) and coarse multi-domain (e.g. >5 μm in magnetite) grains per unit mass.
Frequency-dependent magnetic susceptibility (χ_{FD})	10^{-8} m^3/kg	Indicates levels of superparamagnetic ferrimagnetic grains. These fine magnetic grains can form pedogenically in well-drained and buffered near-surface soil horizons, and their concentrations generally increase with increasing annual rainfall (e.g. Maher et al., 2003a).
Anhysteretic remanent magnetisation (χ_{ARM})	10^{-8} m^3/kg	Primarily sensitive to ferrimagnetic grains in the single domain size range (~25–100 nm), including pedogenic grains, the concentrations of which often increase with increasing annual rainfall.
χ_{ARM}/χ_{FD}	–	Relative proportion of single domain and superparamagnetic ferrimagnetic grains.
χ_{ARM}/SIRM	10^{-3}/Am	Ferrimagnetic grain size, especially the contribution of ferrimagnetic grains in the single domain size range. In soils, values tend to increase with greater pedogenesis and secondary ferrimagnetic mineral formation.
χ_{ARM}/χ_{LF}	–	Ferrimagnetic grain size, especially the contribution of ferrimagnetic grains in the single domain size range. In soils, values tend to increase with greater pedogenesis and secondary ferrimagnetic mineral formation.
Hematite/(hematite + goethite)	–	Relative proportion of hematite to goethite. Hematite formation is favoured in seasonally dry (<~600 mm/yr) and warm environments, whilst goethite formation tends to occur under wetter (>~600 mm/yr) and cooler conditions.

consistent with the stratigraphy, and indicate that the succession formed between at least 44 ka and ~0.83 ka. Fig. 5 presents an age–depth plot of the OSL chronology, which shows that the OSL ages increase relatively uniformly with increasing depth and thus indicate a fairly steady average sedimentation rate of ~0.15 mm/yr. Extrapolating this average sedimentation rate back in time, the lowermost magnetic/DRS sample (collected at 6.6 m depth, 0.4 m below the lowermost OSL sample) can be dated to ~46 ka.

From a nearby section, and using single samples, Tooth et al. (2013) reported OSL ages of 42 ± 2 ka and 32 ± 2 ka for the lower grey palaeosol and lower-middle portions of the red palaeosol, respectively, which agree closely with the ages reported here for the equivalent palaeosols (Figs. 4–5). The OSL ages are also broadly supported by the archaeology hosted within the succession, with Middle Stone Age (>25 ka) artefacts present in the lower grey palaeosol and the lower portions of the red palaeosol and Later Stone Age (<25 ka) artefacts present in the upper portion of the red palaeosol, the upper grey palaeosol and the brown palaeosol (J. Brink, pers. comm.).

4.2. Mineral magnetic and DRS properties

Fig. 6 shows the mineral magnetic and Hm/(Hm + Gt) ratio profiles for the overbank succession, which display variation both within and between palaeosols. Low-frequency magnetic susceptibility (χ_{LF}) is generally low in the lower grey palaeosol (~46–40 ka), with minimum values occurring near the transition to the red palaeosol. From the base of the red palaeosol, values progressively increase upwards, but upon transition to the upper grey palaeosol at ~20 ka, values decline until ~15.5 ka. This is followed by an overall increase in values up through the upper grey and brown palaeosols until ~0.83 ka. This rise in values is especially pronounced in the Holocene-age brown palaeosol, with peak values for the entire succession occurring in the uppermost brown palaeosol. Anhysteretic remanent magnetisation (χ_{ARM}) displays a parallel trend to χ_{LF}. Frequency-dependent magnetic susceptibility (χ_{FD} and χ_{FD}%) also displays a similar trend to χ_{LF}, except for the fact that the decline in χ_{LF} values between ~19.5 and ~15.5 ka starts earlier at ~28 ka. χ_{FD}% values are highest in the brown (mainly 5–8%) and red (mainly 4–6%) palaeosols and lower in the upper and lower grey palaeosols (mainly <4%). χ_{ARM}/χ_{LF} closely parallels χ_{LF}, whilst χ_{ARM}/SIRM shows a distinct peak in the brown palaeosol. In contrast, χ_{ARM}/χ_{FD} shows a broadly opposite trend to many of the magnetic parameters.

Hm/(Hm + Gt) ratios are variable in the lower grey palaeosol, with a sharp peak in values at ~42 ka. From low values at ~41 ka, Hm/(Hm + Gt) ratios generally increase until ~28 ka, but there is then another pronounced decline in values until ~15.5 ka. Similar to many of the magnetic parameters, Hm/(Hm + Gt) ratios then increase from ~15.5 ka until ~0.83 ka. In fact, from ~28 ka until ~0.83 ka, Hm/(Hm + Gt) ratios and χ_{FD}% values show broadly parallel trends ($R^2 = 0.75$).

5. Interpretation

5.1. Overbank sedimentation and palaeosol development (~46 to ~0.83 ka)

The OSL chronology indicates that the overbank succession began accreting prior to ~44 ka and continued until ~0.83 ka. At the study section, the lack of exposure of the basal portions of the lower grey palaeosol means that the age of the onset of overbank

Table 3
Results of OSL analyses for samples from the Modder River overbank succession.

Laboratory code	Depth below surface (m)	H_2O (%)[a]	K (%)	U (ppm)	Th (ppm)	Cosmic ray dose rate (Gy/ka)	Total dose rate (Gy/ka)	n[b]	σ_{OD} (%)[c]	D_e (Gy)[d]	Age (ka)[e]
157/MDER10	0.30	4.0	1.04 ± 0.09	3.78 ± 0.29	6.20 ± 0.94	0.27 ± 0.01	2.24 ± 0.11	95	108	1.87 ± 0.18	0.83 ± 0.09
157/MDER11	0.90	3.8	1.31 ± 0.09	3.04 ± 0.25	6.22 ± 0.81	0.19 ± 0.02	2.22 ± 0.10	41	46	14.0 ± 1.35	6.32 ± 0.67
157/MDER12	1.60	5.0	1.36 ± 0.10	3.04 ± 0.31	7.02 ± 1.00	0.20 ± 0.01	2.32 ± 0.11	41	29	26.2 ± 1.95	11.3 ± 0.98
157/MDER13	3.00	5.1	1.35 ± 0.10	3.50 ± 0.28	6.17 ± 0.90	0.17 ± 0.01	2.32 ± 0.10	41	17	45.4 ± 1.33	19.5 ± 1.04
157/MDER14	3.40	5.8	1.20 ± 0.09	2.62 ± 0.26	5.77 ± 0.84	0.16 ± 0.01	1.99 ± 0.09	39	22	39.8 ± 1.55	20.0 ± 1.19
170/MDER15	3.90	6.7	0.97 ± 0.11	3.32 ± 0.39	5.48 ± 1.27	0.16 ± 0.01	1.92 ± 0.10	30	22	54.1 ± 2.42	28.1 ± 1.93
157/MDER16	4.60	6.2	1.15 ± 0.08	2.65 ± 0.23	5.69 ± 0.76	0.14 ± 0.01	1.94 ± 0.09	45	30	62.5 ± 1.89	32.2 ± 1.74
157/MDER17	4.90	6.0	1.26 ± 0.09	3.38 ± 0.28	5.93 ± 0.92	0.14 ± 0.01	2.18 ± 0.10	39	19	89.1 ± 2.91	40.1 ± 2.30
170/MDER18	6.20	6.7	1.43 ± 0.13	2.84 ± 0.46	9.62 ± 1.53	0.12 ± 0.01	2.41 ± 0.13	44	29	105 ± 5.40	43.5 ± 3.18

[a] Measured field water content. For environmental dose rate calculation, a mean water content value since burial of 15 ± 5% was used.
[b] Number of aliquots used in age calculation. For sample MDER10, single-grain measurements were used for age determination (see text for explanation).
[c] Overdispersion parameter.
[d] D_e values for MDER10 and 11 were calculated using the Minimum Age Model, whilst the Central Age Model was used for all other samples.
[e] Ages are given relative to the measurement date of AD 2011.

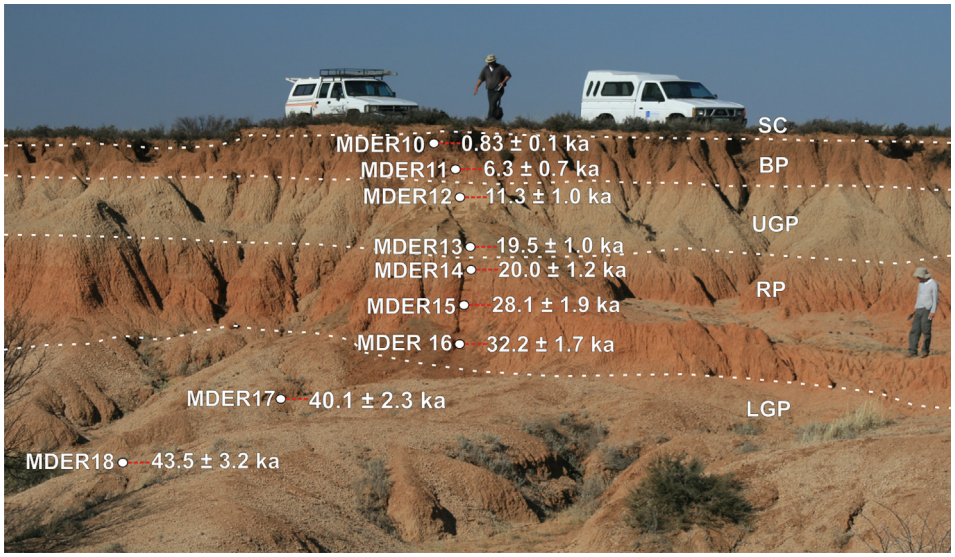

Fig. 4. OSL chronology for the overbank succession at Erfkroon (SC = sandy cap; BP = brown palaeosol; UGP = upper grey palaeosol; RP = red palaeosol; LGP = lower grey palaeosol). In a previous study, Tooth et al. (2013) determined an OSL age of 0.39 ± 0.03 ka for a unit equivalent to the SC (silty sand channel fill) (Fig. 2B). Dashed lines denote the approximate contacts between the palaeosols, although the contacts tend to be gradational. The photograph is looking east with the Modder River to the south. (For interpretation of the references to colour in this figure legend, the reader is referred to the web version of this article.)

sedimentation is unknown, but this effectively marked a shift in the sedimentary regime of the middle Modder River from a relatively high energy, dominantly laterally-migrating system depositing predominantly coarse bedload material, to a lower energy, vertically aggrading system depositing much finer (sandy mud to muddy sand) overbank alluvium (Tooth et al., 2013).

The approximately uniform increase in OSL age with increasing depth (Fig. 5) and the lack of stratigraphic evidence for phases of cut-and-fill prior to ~0.83 ka (Tooth et al., 2013) suggests that the overbank succession accreted at a fairly steady rate (average sedimentation rate = 0.15 mm/yr), with no prolonged breaks in sedimentation or significant phases of erosion. In general, this suggests that pedogenesis operated contemporaneously with sedimentation on a steadily aggrading floodplain surface, rather than during prolonged periods of non-sedimentation. The stacked palaeosols thus appear to be accretionary in nature (cf. Maher et al., 2003b in the context of Chinese loessic palaeosols) and represent a broadly continuous record of overbank sedimentation and contemporaneous pedogenesis from >44 ka to ~0.83 ka. The continuity of the record and accretionary nature of the stacked palaeosols has important implications for use of the magnetic and DRS results as proxies for palaeoclimatic change (see below). After ~0.83 ka, the Modder River deeply incised, effectively terminating this long phase of overbank sedimentation. Incision and donga formation was followed by a phase of channel and donga aggradation involving the deposition of silty sand fills and the silty sand cap (Fig. 2B), before a second phase of deep incision occurred to result in renewed donga formation and exposure of the overbank succession (Tooth et al., 2013).

5.2. Mineral magnetic and DRS properties

The depth plots (Fig. 6) show that the brown palaeosol and the middle to upper portions of the red palaeosol are magnetically enhanced relative to the lower and upper grey palaeosols, an observation that can be ascribed to the neoformation of ultrafine (SP and SD) pedogenic ferrimagnetic magnetite/maghemite (Zhou et al., 1990; Maher et al., 2003a). For example, as shown in Fig. 7A, changes in χ_{LF} are closely linked with changes in χ_{ARM} ($R^2 = 0.87$), and hence concentrations of SD magnetite/maghemite (see Table 2 for an explanation of the parameters). However, the positive *x*-axis intercept of the regression line in Fig. 7A points to the presence of an additional coarser pseudo-single-domain/multi-domain (>~100 nm) background lithogenic ferrimagnetic component.

To explore possible relationships between hematite and goethite and magnetite/maghemite content, Fig. 7C and D show Hm/(Hm + Gt) ratios plotted against χ_{ARM}/χ_{FD} and χ_{FD}%, respectively. Given that the χ_{ARM}/χ_{FD} quotient decreases as the proportion of SP ferrimagnetic grains increases relative to SD grains, the statistically significant negative relationship with Hm/(Hm + Gt)

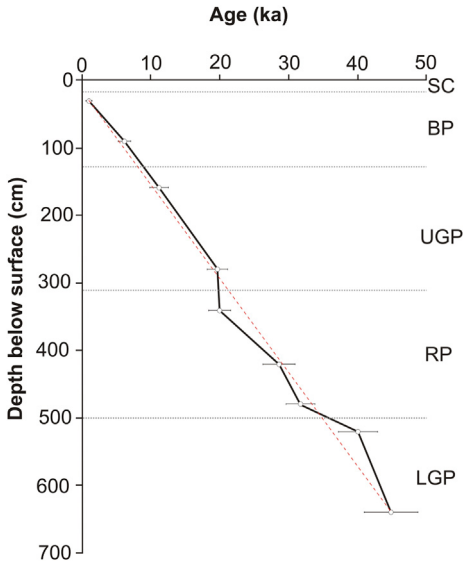

Fig. 5. Age–depth plot for the OSL samples (central age and 1 sigma errors) at Erfkroon (SC = sandy cap; BP = brown palaeosol; UGP = upper grey palaeosol; RP = red palaeosol; LGP = lower grey palaeosol). The red dashed line denotes the average sedimentation rate (~0.15 mm/yr) for the entire timeframe. Horizontal dotted lines denote the approximate contacts between the palaeosols.

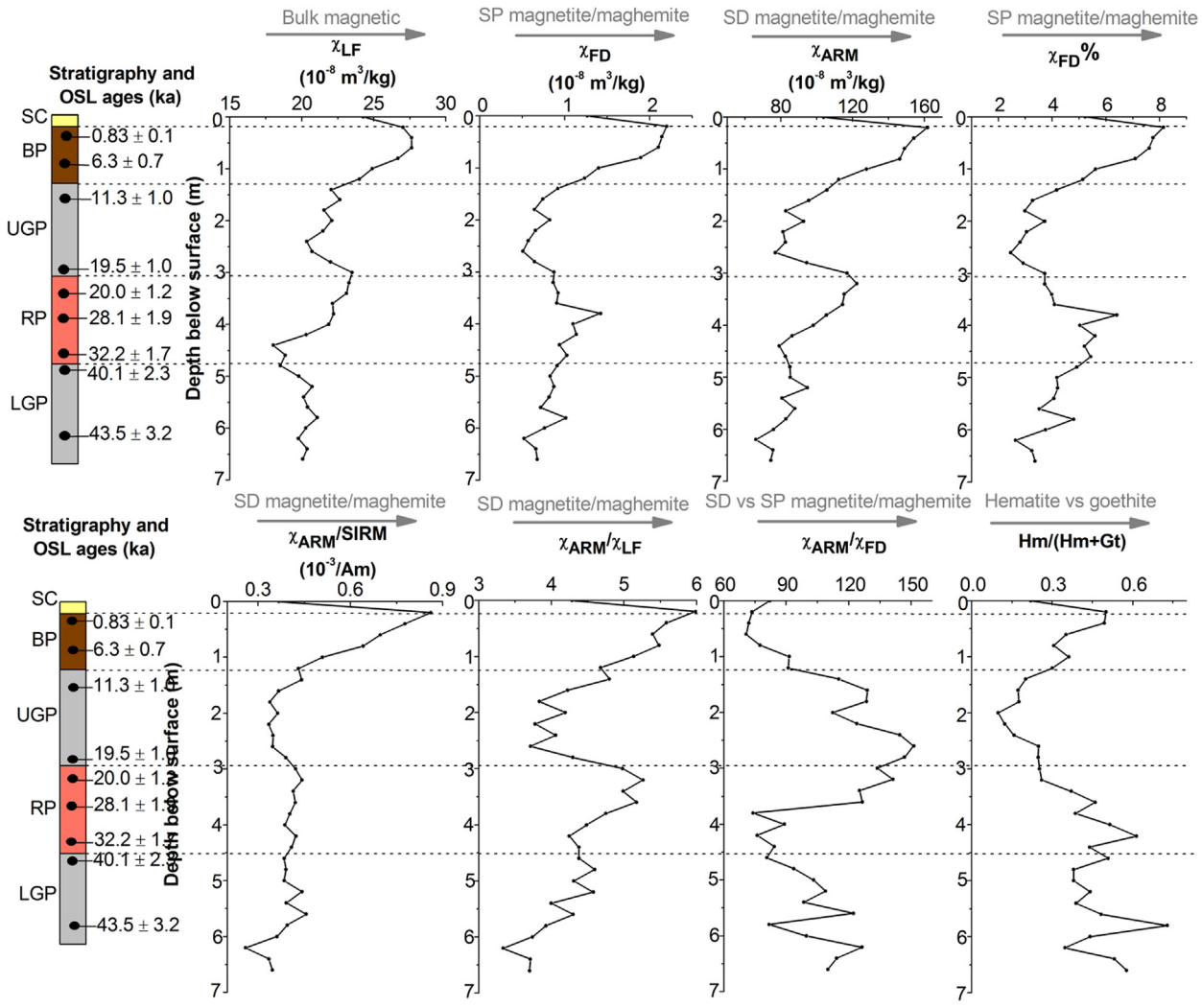

Fig. 6. Stratigraphic column and OSL ages for the overbank succession at Erfkroon (SC = sandy cap; BP = brown palaeosol; UGP = upper grey palaeosol; RP = red palaeosol; LGP = lower grey palaeosol), along with a selection of magnetic parameters that are especially sensitive to the concentration (χ_{LF}, χ_{ARM}, χ_{FD}) or grain size distribution (χ_{FD}%, χ_{ARM}/χ_{FD}, χ_{ARM}/SIRM, χ_{ARM}/χ_{LF}) of ultrafine SP and SD secondary ferrimagnetic minerals. Hm/(Hm + Gt) ratio values derived from DRS measurements are also shown. Horizontal dotted lines denote the approximate contacts between palaeosols, although the contacts are in fact gradational. The general interpretation of the parameters is indicated (see Table 2 for further details). Overall, increasing values for the magnetic parameters points to the enhanced pedogenic formation of fine ferrimagnetic magnetite/maghemite. (For interpretation of the references to colour in this figure legend, the reader is referred to the web version of this article.)

($R^2 = -0.61$) suggests that hematite content tends to increase as levels of SP magnetite/maghemite increase. Similarly, given that χ_{FD}% is sensitive to levels of SP magnetite/maghemite, the positive correlation ($R^2 = 0.50$) between Hm/(Hm + Gt) and χ_{FD}% is also consistent with this relationship. For plots 7C and D, samples from the lower grey palaeosol were excluded because the pedogenic magnetite/maghemite and hematite content of these samples is not consistent with the inferred model of mineral transformation outlined below. The polynomial fit of the data in Fig. 7D also tentatively suggests that once χ_{FD}% values exceed ~6%, SP magnetite/maghemite continues to increase whilst hematite levels start to plateau or even decline slightly.

The statistically significant relationship of Hm/(Hm + Gt) against χ_{ARM}/χ_{FD} and χ_{FD}% suggests that hematite formation is linked with the pedogenic formation of SP magnetite/maghemite. This relationship is consistent with previous observations that pedogenic hematite and maghemite may form concomitantly in aerobic soils through the mineral transformation pathway of ferrihydrite→ SP maghemite→ hematite (Barrón and Torrent, 2002; Torrent et al., 2006). Substantiating these claims, however, will require a firmer understanding of the mineralogy of the pedogenic ferrimagnetic component.

5.3. Controls on palaeosol development and their magnetic and DRS properties

To understand the environmental factors controlling the development of the accretionary palaeosols and particularly acquisition of their magnetic and DRS properties, it is necessary to consider the key soil-forming factors outlined by Jenny (1941): time, topography, parent material and climate (and its co-variant, organic activity). In light of the OSL-based evidence for a fairly steady sedimentation rate and contemporaneous soil development (Fig. 5), soil-forming duration (time) appears not to have varied significantly and thus is unlikely to have been a key determinant of the magnetic and DRS properties. This interpretation is supported by the fact that there is no relationship between the average sedimentation rate between each OSL age and the degree of soil development (magnetic enhancement) inferred from the mineral magnetic data. In turn, this suggests that there was sufficient time

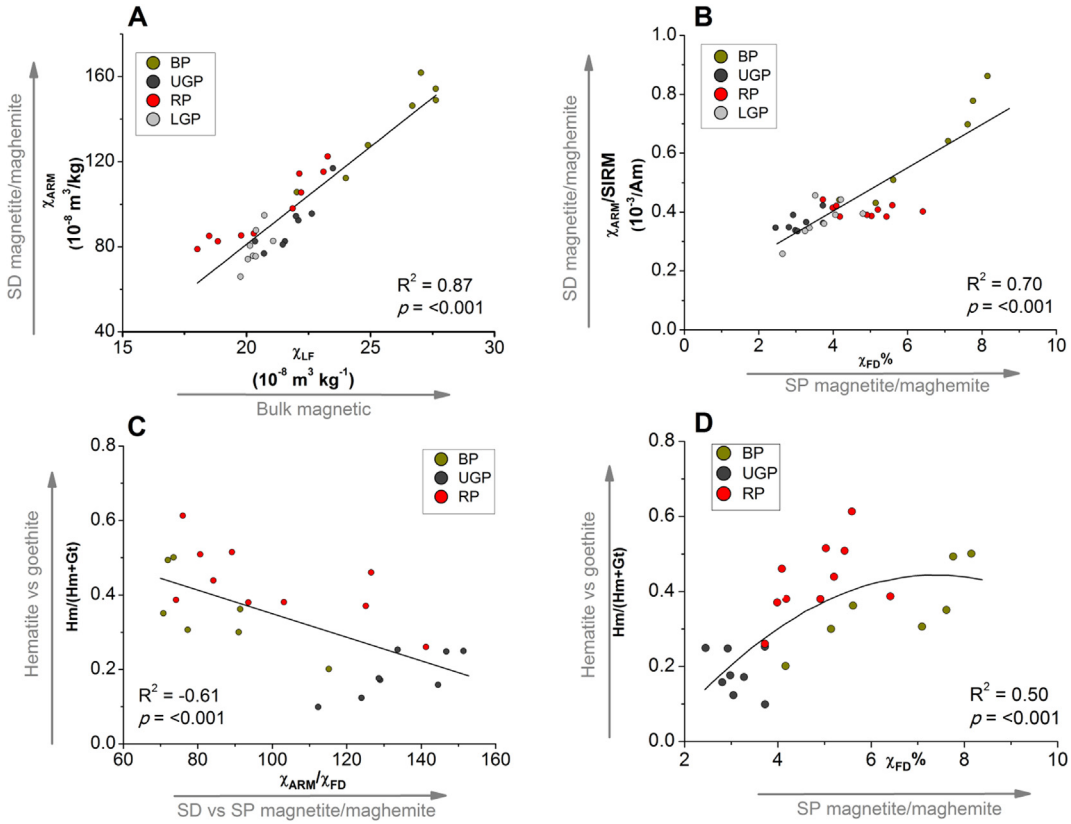

Fig. 7. Plots showing: A) Anhysteretic remanent magnetisation (χ_{ARM}) versus low-frequency magnetic susceptibility (χ_{LF}); B) The ratio of χ_{ARM} to saturation isothermal remanent magnetisation (SIRM) versus frequency-dependent magnetic susceptibility (χ_{FD}%); C) Hm/(Hm + Gt) versus χ_{ARM}/χ_{FD}; and D) Hm/(Hm + Gt) versus χ_{FD}%. In plots C and D, samples from the lower grey palaeosol are excluded since these samples appear not to be consistent with the inferred model of magnetic enhancement (see text for explanation). The general interpretation of each parameter is shown. The regression lines can also be seen as pedogenic intensity gradients, with higher levels of SP and SD magnetite/maghemite and Hm/(Hm + Gt) ratios generally indicating more intense pedogenesis (BP = brown palaeosol; UGP = upper grey palaeosol; RP = red palaeosol; LGP = lower grey palaeosol). (For interpretation of the references to colour in this figure legend, the reader is referred to the web version of this article.)

for the iron oxide assemblages in surface soil horizons to reach steady-state equilibrium with climatic conditions, which is crucial for interpreting the magnetic and DRS data at different depths as 'snapshots' of palaeoclimatic conditions (Maher and Thompson, 1995). Moreover, with respect to the Hm/(Hm + Gt) ratio, previous studies of soil chronosequences in a variety of settings have shown the ratio of pedogenic hematite to goethite to be largely independent of the duration of soil development (Torrent, 1976; Torrent et al., 1980).

The 'layer cake' stratigraphy at the study section (Figs. 2B and 4) also indicates that the gradients (topography) of the floodplain surface remained subdued throughout overbank sedimentation. Source lithology (parent material) is also unlikely to have changed significantly over time (e.g. from dominantly sedimentary to igneous lithologies), because the catchment upstream of Erfkroon is underlain by shales, siltstones and sandstones, albeit with local dolerite sills and dykes. Hence, given that soil-forming duration, topography and parent material appear to have remained relatively constant over time, we can conclude that climate is left as the most likely chief control on soil development, and thus the main determinant of the temporal trends in magnetic and DRS properties (cf. Maher et al., 2003b).

Two additional factors that may have acted to obscure or compromise the preservation of the climate-related palaeosol magnetic and DRS signals, however, are: i) sediment mixing (e.g. through bioturbation); and ii) fluctuations in the level of the water table in this floodplain setting. Tooth et al. (2013) noted evidence for bioturbation and pedoturbation in the palaeosols (e.g. minor tube-like structures, slickensides). However, the magnetic data are not consistent with the occurrence of significant sediment mixing, since this would tend to lead to a more homogenous magnetic profile (Lindquist et al., 2011) and mean that the distinct temporal variations in magnetic properties displayed in Fig. 6 would not have been preserved. The single-grain OSL data for the near-surface sample (MDER10) also supports this interpretation. Significant sediment mixing (bioturbation) in such a relatively young (~0.83 ka) soil/palaeosol sample would tend to lead to the presence of zero-dosed grains, as grains at the surface are bleached and subsequently translocated deeper into the soil profile (Bateman et al., 2003, 2007), but zero-dosed grains have not been detected in this sample (Fig. 3C). The available evidence also suggests that the mineral magnetic and DRS records were not affected by prolonged waterlogging (i.e. by a perched or elevated water table), because this too would tend to result in a more homogenous magnetic profile due to the dissolution of pedogenic SP and SD ferrimagnetic grains (found particularly in the red and brown palaeosols) under persistently anoxic conditions (Maher, 1998). Overall, it appears that palaeoclimatic changes during the formation of the overbank succession had limited bearing on the rate of sedimentation, but instead were imprinted in the pedological properties of the palaeosols, including iron oxide assemblages.

Given that OSL dating determines when sediment was deposited, using the OSL ages to provide a chronology for the mineral magnetic and DRS profiles is reliant on minimal delay between overbank sedimentation and subsequent pedogenesis, including the acquisition of the magnetic and DRS signal. The sample at 0.3 m

depth (Table 3) can be used to assess the likely time lag between these processes. Since this sample was deposited at ~0.83 ka, and much of the silty sand deposit that caps the brown palaeosol (Fig. 2B) had been deposited by ~0.39 ka (i.e. contemporaneously with the deposition of the silty sand channel fill – Tooth et al., 2013), the acquisition of the magnetic and DRS signal in the brown palaeosol must have occurred within ~420 years. If this timeframe for soil development is deemed to be broadly representative of the entire overbank succession, which is plausible given the apparent slow and fairly steady sedimentation rate (Fig. 5), then the lag between sediment deposition and the acquisition of the magnetic and DRS signal may have been less than a few hundred years. This finding supports the use of the OSL ages as a chronologic framework for interpretation of the palaeoclimatic significance of the magnetic and DRS profiles, especially given that this timeframe for the acquisition of iron oxide assemblages is, with the exception of MDER10, less than the one sigma error estimates for the OSL ages (Table 3).

6. Discussion

Pedogenesis in well-drained soils commonly results in the magnetic enhancement of near-surface soil layers through the neoformation of ultrafine SP and SD magnetite/maghemite. These secondary magnetic minerals may originate from a variety of biotic (Guyodo et al., 2006) and abiotic (Maher and Taylor, 1988; Barrón and Torrent, 2002) processes. Studies of surface soils in a range of climatic environments have demonstrated that pedogenic enhancement generally increases as annual rainfall increases (Balsam et al., 2011). In particular, the pedogenic formation of SP and SD magnetite/maghemite has been found to be greatest in soils that experience seasonal wetting and drying in Mediterranean, monsoonal and tropical wet-dry climates (Tite and Linington, 1975; Balsam et al., 2011). As annual rainfall exceeds around 1200–1500 mm/yr, however, the level of soil magnetic enhancement diminishes as increasing soil saturation results in the reductive dissolution of ferrimagnetic minerals and the formation of reduced forms of iron (e.g. iron sulphides) (Balsam et al., 2011; Long et al., 2011). The χ_{FD}% parameter has been widely used as an indicator of the significance of the SP grain size fraction to determine changes in the intensity of pedogenesis and its relationship to rainfall (e.g. Maher and Thompson, 1995; Maher et al., 2003a). Typically, χ_{FD}% values from 5 to 8% indicate the presence of elevated levels of pedogenic SP magnetite/maghemite (Liu et al., 2007).

Hematite and goethite are common constituents of soils. Hematite and goethite ratios have been used to reconstruct changing palaeoclimatic conditions from palaeosols (Balsam et al., 2004; Ji et al., 2004; Torrent et al., 2007), because these iron oxides are generally associated with contrasting climatic conditions (Schwertmann and Taylor, 1989). Hematite formation is favoured by warmer, drier and more seasonal climatic conditions, especially where seasonal rainfall is between around 200 and 600 mm/yr (Schwertmann, 1985). Hematite formation is at its maximum when high temperatures coincide with a short wet season (period of soil wetting), which is then followed by an extended dry season (period of soil oxidation). As the length of the wet season increases, hematite formation plateaus and soon declines rapidly as the period for oxidation diminishes. In contrast, goethite formation is favoured by cooler, wetter and less seasonal climatic conditions, when soil saturation becomes more likely (Kämpf and Schwertmann, 1983). Indeed, Long et al. (2011) found Hm/(Hm + Gt) ratios for modern soils along a rainfall transect in south China to systematically decrease with increasing rainfall ($R^2 = -0.87$). In general, the pedogenic formation of both magnetite/maghemite and hematite increases between around 200 and 600 mm/yr, but above 600 mm/yr pedogenic magnetite/maghemite formation continues to increase whilst hematite declines (Balsam et al., 2004).

Pedogenic (secondary) calcium carbonate ($CaCO_3$) and gypsum ($CaSO_4.2H_2O$) are also common constituents of dryland soils, and are present in the Erfkroon palaeosols (Table 1). Pedogenic carbonate (excluding groundwater-derived carbonate) generally forms in environments where the climate is seasonally to mostly dry, with seasonal rainfall between ~100 and 500 mm/yr (Goudie, 1983; Birkeland, 1999; Tanner, 2010). Gypsum tends to form where mean monthly potential evaporation exceeds mean monthly rainfall throughout the year and is thus restricted to hyperarid, arid and semi-arid environments where annual rainfall is less than ~400 mm/yr (e.g. Watson, 1985).

6.1. Palaeoclimatic changes at Erfkroon from ~46 to ~0.83 ka

Based on the links between pedogenic constituents (iron oxides, calcium carbonate and gypsum) and climate outlined above, below we propose a three phase model of climate change during the last ~46 ka at Erfkroon. In terms of iron oxide content, we focus on the use of χ_{FD}% and Hm/(Hm + Gt) ratios. The χ_{FD}% parameter is used as a proxy for the intensity of pedogenesis, and as in previous studies, we interpret this parameter to be controlled by climate and principally rainfall (see above). Interestingly, χ_{FD}% values display a statistically significant correlation ($R^2 = 0.61$, $p < 0.0001$) with the last ~46 ka of the Lake Tswaing (Fig. 1) palaeorainfall record (Partridge et al., 1997) (Fig. 8). The inferred relationship between sediment grain size and mean annual precipitation on which the Lake Tswaing palaeorainfall record is based, however, has been questioned (e.g. Chase et al., 2010). Although the correlation between the Erfkroon and Lake Tswaing records does not necessarily confirm the interpretation of either proxy, it does nonetheless suggest that the proxies are controlled by a common climatic forcing mechanism.

The Hm/(Hm + Gt) ratio is likely to be controlled by a combination of rainfall and temperature (Kämpf and Schwertmann, 1983). However, given that we attribute changes in χ_{FD}% primarily to changes in rainfall, the relationship between χ_{FD}% and Hm/(Hm + Gt) shown in Fig. 7D suggests that rainfall is also a primary determinant of the Hm/(Hm + Gt) ratios, at least for the record spanning the red, upper grey and brown palaeosols (Fig. 6). Where available, Southern Hemisphere (ice and marine core) and southern African terrestrial proxy records are drawn upon to support our interpretations (Fig. 9; see Fig. 1 for the location of terrestrial proxy records discussed). We also propose tentative estimates of palaeorainfall at Erfkroon based on the rainfall-dependence of pedogenic magnetite/maghemite, hematite, goethite, calcium carbonate and gypsum formation outlined above.

Phase 1 (~46–28 ka): From ~46 to 41 ka, χ_{FD}% values (≤3%) indicate that levels of SP magnetite/maghemite are low and comparable to minimum values in the upper grey palaeosol (see below). In contrast, Hm/(Hm + Gt) ratios are comparatively high (mostly ≥0.4) (Fig. 9A and B). Combined, this suggests that temperatures were sufficiently warm and seasonal precipitation high enough to promote hematite formation, but precipitation was still too low for significant SP magnetite/maghemite production. The presence of large pedogenic calcium carbonate nodules and disseminated gypsum within this palaeosol is also consistent with dry conditions. Together, this evidence suggests that seasonal rainfall was probably between 200 and 400 mm/yr. The only exception to this is a sharp peak at ~42 ka in the Hm/(Hm + Gt) ratio, which represents the highest value for the entire record, and an associated smaller peak in χ_{FD}% (5%). This points to an abrupt and short lived increase in annual rainfall (but remaining seasonal) at ~42 ka, although rainfall is unlikely to have significantly exceeded ~600 mm/yr

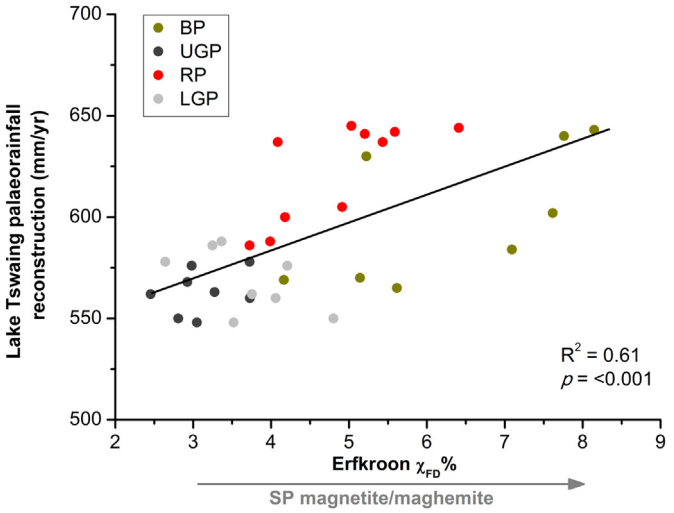

Fig. 8. Plot of frequency-dependent magnetic susceptibility (χ_{FD}%) for the overbank succession at Erfkroon (BP = brown palaeosol; UGP = upper grey palaeosol; RP = red palaeosol; LGP = lower grey palaeosol) versus the palaeorainfall record from Lake Tswaing (Partridge et al., 1997). (For interpretation of the references to colour in this figure legend, the reader is referred to the web version of this article.)

since hematite formation tends to decline above this level. The Lake Tswaing palaeorainfall record also indicates a brief increase in rainfall at ~42 ka (Fig. 9C).

From ~41 to 28 ka, concentrations of SP magnetite/maghemite and Hm/(Hm + Gt) ratios increased, which suggests that the climate became wetter and possibly warmer over this period. Elevated levels of SP magnetite/maghemite (χ_{FD}% = 5–7%) are particularly apparent in the red palaeosol from ~32 to 28 ka. This magnetic enhancement corresponds with a period of inferred increase in annual rainfall recorded at Lake Tswaing (Fig. 9C), as well as evidence for widespread increased humidity in the Kalahari over the same time period (Chase and Meadows, 2007 and references therein). Sea-surface temperatures (SSTs) in the SW Indian Ocean are considered to be a key determinant of moisture supply to the summer rainfall zone (SRZ, see Fig. 1) by controlling the evaporation and transport of moisture to the interior via tropical easterly circulation, both at present (e.g. Goddard and Graham, 1999) and over multi-millennial timescales (e.g. Dupont et al., 2011). Increased rainfall at Erfkroon from ~32 to 28 ka, however, shows no clear correspondence with SW Indian Ocean SSTs (Fig. 9D). An alternative explanation is proposed by Chase and Meadows (2007), who suggest that increased humidity in the Kalahari between ~32 and 28 ka may have been linked to: 1) the occurrence of obliquity and Southern Hemisphere insolation minima at ~29 ka and ~32 ka, respectively (Fig. 9F and G), during a general 100 ka cycle of glacial development; and 2) the resulting expansion of Antarctic sea ice, the equatorward migration and intensification of westerly (Atlantic Ocean) rain-bearing circulation systems (Stuut et al., 2004; Chiang and Bitz, 2005), and the expansion of the winter rainfall zone (WRZ, see Fig. 1) into the interior of southern Africa. This inferred equatorward shift of the westerlies may also be reflected in the cooling of Agulhas waters and/or reduced water exchange between the Indian and Atlantic oceans at around 30 ka (Peeters et al., 2004; Martínez-Méndez et al., 2010). Moreover, the close coupling between climatic changes at Erfkroon and the Lake Tswaing palaeorainfall record (Fig. 8) implies that westerly moisture flux from the Atlantic Ocean may even have affected north-eastern areas of South Africa during this period. This orbitally-forced mechanism of enhanced winter rainfall provides a plausible explanation for increased rainfall at Erfkroon during this latter part of Phase 1, and perhaps further afield, but the notion of an expanded WRZ during the Last Glacial cycle remains contentious (cf. Lee-Thorp and Beaumont, 1995; Gasse et al., 2008) and further robust proxy records are needed to validate this mechanism.

Phase 2 (~28–15.5 ka): χ_{FD}% values show that concentrations of SP magnetite/maghemite consistently decline from ~28 to 15.5 ka, which is paralleled by a decline in Hm/(Hm + Gt) ratios (Fig. 9A and

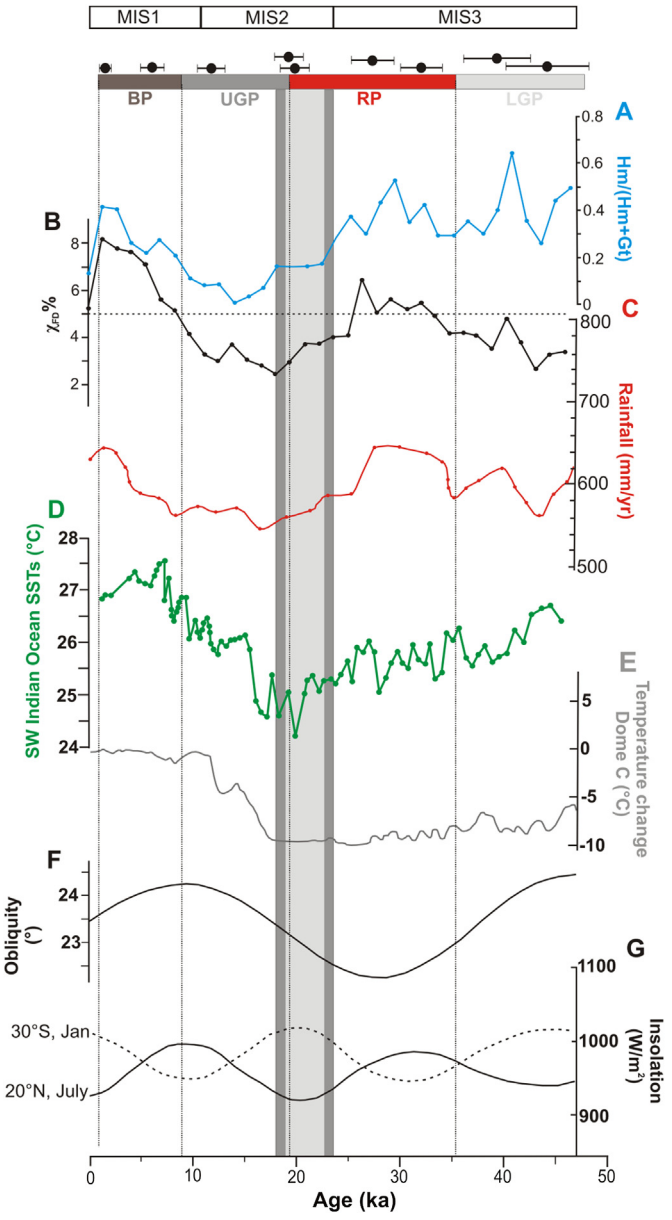

Fig. 9. Comparison of select records from the overbank succession at Erfkroon with a range of Southern Hemisphere and southern African palaeoenvironmental records: (A) Hm/(Hm + Gt) ratios; (B) frequency-dependent magnetic susceptibility (χ_{FD}% – the horizontal dashed line at 5% is shown to highlight that values ≥5% typically indicate the significant presence of pedogenic SP magnetite/maghemite); C) Lake Tswaing palaeorainfall record (Partridge et al., 1997); D) reconstructed SW Indian Ocean sea-surface temperatures (core MD79257; Bard et al., 1997; Sonzogni et al., 1998); and E) temperature variations at Dome C Antarctica (Jouzel et al., 2007). Obliquity (F) and insolation (G) curves are also shown. The light and dark vertical grey bars denote the LGM as defined by Gasse et al. (2008) and Chase and Meadows (2007), respectively, in their syntheses of southern African late Quaternary climatic change. The palaeosol units and OSL ages (including their one sigma errors) of the succession at Erfkroon are shown at the top of the diagram, as well as the boundaries of Marine Isotope Stages (MIS) 1–3.

B). This time period includes the upper portions of the red palaeosol and the lower to middle portions of the upper grey palaeosol. Typically, low Hm/(Hm + Gt) values indicate the enhanced presence of goethite relative to hematite. In this instance, however, the decline in Hm/(Hm + Gt) values over this time period is inferred to reflect a shift towards increasingly cooler and drier conditions, under which both hematite and goethite formation is inhibited. This interpretation is consistent with: 1) the parallel decline in levels of pedogenic magnetite/maghemite (χ_{FD}%), the formation of which is also inhibited by dry conditions; 2) the presence of calcium carbonate nodules and gypsum, the latter being particularly abundant around the red/upper grey palaeosol transition at ~20 ka (Table 1); and 3) the parallel decline in annual rainfall recorded at Lake Tswaing (Partridge et al., 1997 – Fig. 9C). The decrease in rubification in the transition from the red to the upper grey palaeosol can thus be attributed to a decrease in hematite formation.

The inferred trend towards more arid conditions from ~28 to 15.5 ka corresponds closely with the Lake Tswaing palaeorainfall record, which indicates a decline in rainfall in northeastern South Africa from ~28 ka to a minimum at ~17–18 ka when it was ~15% lower than today (Partridge et al., 1997) (Fig. 9C). In contrast, Chase and Meadows (2007) suggested that a second key phase of enhanced humidity in the Kalahari occurred from ~22 to 17 ka, which they also attributed to an expansion of the WRZ and enhanced moisture supply to the interior via westerly circulation. Based on an interpolation of palaeo-datasets indicating increased humidity, Chase and Meadows (2007) presented a reconstruction of the WRZ expansion during the LGM (Fig. 1). Despite Erfkroon lying within this reconstructed expansion, albeit close to its eastern limit, our data indicate aridity during and slightly after the LGM. The record at Erfkroon thus provides further insight into the possible eastern extent of the WRZ during the LGM. Dry conditions at this time were probably caused by limited supply both of easterly summer and westerly winter moisture, as well as a more northerly position of the intertropical convergence zone (ITCZ). At Alexandersfontein, however, situated ~80 km west of Erfkroon (Fig. 1), evidence for high lake levels between 19.3 and 17 ka has been interpreted to indicate that annual rainfall was about twice that of today (Butzer et al., 1973; Butzer, 1984). Clearly, further research is needed in this region of interior South Africa to elucidate the dynamics of the WRZ during the Quaternary.

SP magnetite/maghemite and Hm/(Hm + Gt) ratios are at their lowest for the entire record between ~18 and 15.5 ka. Rainfall during this period is likely to have been <400 mm/yr, and probably as low as 100–200 mm/yr. This level of rainfall is too low for significant SP magnetite/maghemite and hematite formation, but sufficient for pedogenic calcium carbonate and gypsum formation (Table 1). This interpretation is consistent with a stable nitrogen isotope and amino acid racemization record from ostrich eggshells at Equus Cave ~170 km northwest of Erfkroon, which indicates that mean annual rainfall was 190 ± 50 mm/yr at 17 ka (Johnson et al., 1997). Rainfall at Erfkroon was probably at its lowest at ~18–15.5 ka, which corresponds with Heinrich event 1 (H1, 18–15 ka) when large amounts of ice and meltwater entered the North Atlantic (e.g. Bond et al., 1992). In a review of palaeo-datasets, mainly across Africa and Asia, Stager et al. (2011) presented evidence for severe aridity during H1 affecting much of the monsoon region of Africa, as well as parts of SE Africa. This includes records from Cold Air Cave (Holmgren et al., 2003) and the Limpopo watershed (core MD96-2048, Dupont et al., 2011). Stager et al. (2011) suggest that aridity during H1 is unlikely to be solely linked to changes in the meridional positioning of the ITCZ, and is also probably controlled by severe weakening of rainfall systems in response to sea surface cooling. Thomas et al. (2012) have questioned this notion of pervasive aridity during H1 in Africa, drawing attention to records not considered by Stager et al. (2011) that indicate wetter conditions and which thus point to greater spatial and temporal climatic complexity. Although the driest conditions at Erfkroon appear to have occurred during H1, it is important to note that this does not represent an abrupt shift to dry conditions, but rather a progressive drying trend that initiated at ~28 ka and continued until ~15.5 ka.

Phase 3 (~15.5–0.83 ka): from ~15.5 to 0.83 ka, χ_{FD}% values and Hm/(Hm + Gt) ratios increase markedly, which indicates an increase in concentrations of SP magnetite/maghemite and hematite content (Fig. 9A and B). This time period encompasses the middle to upper portions of the upper grey palaeosol and all of the brown palaeosol. These data are consistent with rising temperatures and annual (but seasonal) rainfall during the late Pleistocene and through much of the Holocene. A broadly similar trend is recorded in the Lake Tswaing palaeorainfall record (Fig. 9C), which indicates an overall increase in mean annual rainfall from around 17 ka onwards (Partridge et al., 1997). A recent $\delta^{15}N$ record from Lake Tswaing points to increasing rainfall from 16.2 ka, but this inferred increase terminates earlier (at 7.7 ka) than the Lake Tswaing palaeorainfall and Erfkroon records (Schmidt et al., 2014). A quantitative pollen-based palaeoclimate reconstruction from Wonderkrater also indicates general increases in both temperature and rainfall (specifically during the warmest and wettest quarters of the year) from around 17 ka, most notably following the Younger Dryas, with maximum moisture availability at ~3–7 ka (Truc et al., 2013).

The increase in hematite content and inferred rise in temperatures from ~15.5 ka is consistent with Southern Hemisphere and southern African palaeoclimatic records, including the Vostok ice core temperature record (Petit et al., 1999) (Fig. 9E), Stampriet and Uitenhage aquifer $\delta^{18}O$ records (Stute and Talma, 1998), Boomplaas Cave (Thackeray, 1990) and Wonderkrater pollen records (Scott et al., 2003; Truc et al., 2013), and an alkenone-SST reconstruction from the Mozambique Channel (core MD79257, Bard et al., 1997), all of which indicate a dominant trend of postglacial warming from ~17 to 15 ka until around the early to mid Holocene.

Increases in rainfall at Erfkroon are particularly pronounced from the onset of the Holocene. This is an important finding since it is inconsistent with hypotheses that predict drier early Holocene conditions in relation to an austral summer insolation minimum (e.g. Kutzbach, 1981; Marzin and Braconnot, 2009). Enhanced moisture availability during the early to mid Holocene has been inferred from other records from South Africa's SRZ, including stable isotope and greyscale records from Cold Air Cave (Lee-Thorp et al., 2001; Holmgren et al., 2003) and a $\delta^{13}C$ record from Braamhoek wetland (Norström et al., 2009).

The increase in seasonal rainfall at Erfkroon during the deglacial period and through much of the Holocene may at least partly be linked to rising SSTs in the SW Indian Ocean (Bard et al., 1997; Sonzogni et al., 1998 – core MD79257) (Fig. 9D) and the enhanced supply of moisture to southern Africa's SRZ through easterly flow (Jury et al., 2002). The record at Erfkroon thus contributes to a growing body of evidence supporting the notion that deglacial increases in SW Indian Ocean SSTs played a primary role in controlling climates in SE Africa (e.g. Dupont et al., 2011; Stager et al., 2011; Truc et al., 2013; Schmidt et al., 2014), rather than changes in the mean latitudinal position of the ITCZ in response to Northern Hemisphere cold events and direct insolation forcing (e.g. Johnson et al., 2002; Schefuß et al., 2011). The evidence for increasing seasonal rainfall during the Holocene, however, contrasts with some other southern African records indicating a progressive drying trend during the Holocene, although this particularly relates to records in the west of the subcontinent

(Gasse et al., 2008) that include high-resolution stable isotope hyrax midden records from Namibia (Chase et al., 2010). Chase et al. (2010) have suggested that this drying trend during the Holocene is also evident in the Cold Air Cave speleothem record (Holmgren et al., 2003) in northeastern South Africa, but no consensus has emerged as to the interpretation of this record. Contrasting hydroclimatic conditions during the Holocene between western and eastern parts of southern Africa is not surprising given the dynamic interplay of both westerly (Atlantic Ocean) and easterly (Indian Ocean) moisture sources, which may have given rise to a complex mosaic of climatic changes (Burrough and Thomas, 2013).

The highest concentrations of SP magnetite/maghemite occur during the late Holocene ($\chi_{FD}\% = 7–8\%$) at around 0.83 ka. This time corresponds with part of the Medieval Climatic Anomaly (MCA, ~900–1300 AD) when conditions across a wide area of southern Africa's SRZ are generally considered to have been warmer and wetter than at present, albeit variable (e.g. Tyson et al., 2000; Ekblom and Stabell, 2008; Nicholson et al., 2013). Seasonal rainfall at ~0.83 ka is likely to have been around 600–700 mm/yr, as suggested by the significant formation of both SP magnetite/maghemite and hematite (Balsam et al., 2004), the absence of gypsum and the decreased presence of pedogenic calcium carbonate in the upper portions of the brown palaeosol (Table 1). Rainfall at ~0.83 ka was thus higher than the modern rainfall of 400–500 mm/yr. This contrasts with records from the modern WRZ, which indicate generally drier conditions during the MCA (e.g. Stager et al., 2012). A growing body of evidence supports the notion that suborbital climatic variability during the Holocene across southern Africa has been driven by variations in solar activity, including the Spitzkoppe hyrax midden (e.g. Chase et al., 2009) and Cold Air Cave speleothem records (Woodborne et al., 2008).

6.2. *Fluvial geoproxies as sources of palaeoenvironmental data in the drylands of southern Africa*

Geoproxies are a vital source of palaeoenvironmental data in the drylands of interior southern Africa where traditionally favoured organic-based proxies are scarce. To date, the extraction of palaeoenvironmental information from landforms has tended to focus on sand dunes and palaeolake shorelines, yet the interpretation of these records has proved challenging and remains contentious (Chase, 2009; Thomas and Burrough, 2012, in press). Fluvial landforms offer an additional form of geoproxy data, but have received limited research attention. Based on the findings of this study, however, we contend that fluvial geoproxies represent an underutilised source of proxy data and that greater research attention should be directed at fully exploring the palaeoenvironmental signatures contained within fluvial successions. Of course, not all fluvial successions will furnish unambiguous or interpretable records of palaeoenvironmental change, and this is especially true for fluvial systems that have evolved in response to autogenic forcing rather than allogenic climatic forcing (e.g. Tooth et al., 2007). Nevertheless, this study demonstrates the existence of alluvial-palaeosol successions in interior South Africa that can provide relatively long and apparently broadly continuous records of past environmental, and specifically climatic, change. Compared to sand dune and lake shoreline geoproxy datasets, the record at Erfkroon generally offers greater continuity and the palaeoclimatic factors controlling proxy signatures are less ambiguous (cf. Chase, 2009). Moreover, unlike sand dunes and lake shorelines, which can potentially simply record the occurrence of extreme climatic events (Thomas and Burrough, 2012), the record at Erfkroon provides information on more 'average' climatic conditions on centennial to millennial timescales. It is not yet clear just how common such continuous alluvial-palaeosol successions are in southern Africa, and further exploration is needed to try and identify sites similar to Erfkroon. Ultimately, more focused investigation on fluvial geoproxies, especially in arid to semi-arid regions of interior southern Africa, will contribute to enhancing the spatial coverage of robust palaeo-datasets and thus help to develop a clearer picture of the nature, spatial patterns and forcing mechanisms of late Quaternary climatic changes.

This study also highlights the importance of sites where significant geoproxy and archaeological records coincide (Maslin and Christensen, 2007; Thomas and Burrough, 2012), since the palaeoclimatic interpretations presented in this study potentially can be used to explore links between late Quaternary climatic changes and the record of human stone tool technological development during the African Middle Stone Age and Later Stone Age. In many previous studies, interpretations of the links between human evolution, technological development and climatic change have relied on correlation with remote (e.g. ice core and marine) records (e.g. Jacobs et al., 2008; Ziegler et al., 2013), which do not necessarily reflect the complexity of regional patterns of terrestrial change (e.g. Chase, 2010; Burrough and Thomas, 2013).

7. Conclusions

OSL dating of an overbank alluvial succession along the middle reaches of the Modder River in central South Africa indicates that sedimentation initiated prior to 44 ka and continued at a steady average rate of ~0.15 mm/yr until ~0.83 ka. The fairly steady sedimentation rate and lack of evidence for significant phases of erosion during this long time interval suggest that the four stacked palaeosols contained within the succession are accretionary, with pedogenesis having occurred contemporaneously with sedimentation. Taking into consideration the five soil-forming factors outlined by Jenny (1941), climate is identified as the key control on the intensity of pedogenesis. This is reflected in the changing concentration of pedogenic ferrimagnetic minerals (magnetite/maghemite) of single domain and superparamagnetic dimensions, and variations in the amount of hematite compared to goethite. Based on these changes in iron oxide assemblages and other secondary soil constituents (gypsum and calcium carbonate), we identify three key phases of palaeoclimatic change over the past ~46 ka at Erfkroon. The climate was generally dry (rainfall ~200–400 mm/yr) from ~46 to 32 ka, except for a brief peak in humidity at ~42 ka. Humidity was greater (rainfall ~400–600 mm/yr) from ~32 to 28 ka, possibly linked to the equatorward migration and intensification of westerly storm tracks. After ~28 ka, the climate became progressively cooler and drier until ~18–15.5 ka when rainfall was ~100–200 mm/yr. Temperatures and seasonal rainfall increased from ~15.5 to 0.83 ka, which at least until the mid Holocene may have been linked to rising SSTs in the SW Indian Ocean. At ~0.83 ka during the MCA, seasonal rainfall peaked at ~600–700 mm/yr and was higher than at present (~400–500 mm/yr).

The palaeoclimatic changes recorded at Erfkroon bear marked similarity to the Lake Tswaing palaeorainfall record (Partridge et al., 1997), which points to a regionally coherent pattern of rainfall change across central and northeastern South Africa over at least the last ~46 ka. More focused research across interior southern Africa, however, is needed to elucidate the regional expression of this palaeorainfall record and the underlying controls, particularly in relation to changes in the position, intensity and relative importance of westerly (Atlantic Ocean) and easterly (Indian Ocean) circulation systems. Overall, this study provides novel insight into late Quaternary climatic dynamics in a region of interior South Africa where continuous and well-dated proxy records are scarce (Chase and Meadows, 2007; Gasse et al., 2008). More

generally, this study also demonstrates the potential of fluvial geoproxy archives to provide robust palaeo-datasets with generally greater continuity and possibly less ambiguous interpretation than other geoproxies (e.g. sand dunes). Identifying and investigating other sites similar to Erfkroon presents a unique opportunity to develop a new and possibly pervasive source of significant palaeoclimatic data in interior southern Africa. Moreover, the overbank alluvial succession at Erfkroon hosts archaeological remains recording the transition from the African Middle to Later Stone Ages and thus the palaeoclimatic record at this and similar sites may prove useful in exploring climate change as a driver of human technological development.

Acknowledgements

This research was conducted whilst RL was in receipt of a NERC PhD studentship at Aberystwyth University. Additional support was provided by a grant from the Aberystwyth University Research Fund to ST. The authors thank James Brink for help in arranging accommodation and assistance in the field, and Matthew Kitching for arranging the loan of a vehicle and field equipment from the University of the Witwatersrand. Mike O'Connor is thanked for access to the Environmental Magnetism Laboratory at the University of Liverpool and Richard Chiverrell for advice regarding the DRS analyses. We thank the two anonymous reviewers for their constructive comments that helped us to clarify the presentation and interpretations.

References

Adamiec, G., Aitken, M., 1998. Dose-rate conversion factors: update. Anc. TL 16, 37–50.
Alexanderson, H., Murray, A.S., 2007. Was southern Sweden ice free at 19-25 ka, or were the post LGM glacifluvial sediments incompletely bleached? Quat. Geochronol. 2, 229–236.
Balsam, W.L., Ji, J., Chen, J., 2004. Climatic interpretations of the Luochuan and Lingtai loess sections, China, based on changing iron oxide mineralogy and magnetic susceptibility. Earth Planet. Sci. Lett. 223, 335–348.
Balsam, W.L., Ellwood, B.B., Ji, J., Williams, E.R., Long, X., El Hassani, A., 2011. Magnetic susceptibility as a proxy for rainfall: worldwide data from tropical and temperate climates. Quat. Sci. Rev. 30, 2732–2744.
Bard, E., Rostek, F., Sonzogni, C., 1997. Interhemispheric synchrony of the last deglaciation inferred from alkenone palaeothermometry. Nature 385, 707–710.
Barker, C.H., 2011. Utilising published data for DTM construction and drainage basin delineation in the Modder River catchment, Free State, South Africa. South Afr. Geogr. J. 93, 89–103.
BarrÓn, V., Torrent, J., 2002. Evidence for a simple pathway to maghemite in Earth and Mars soils. Geochim. Cosmochim. Acta 66, 2801–2806.
Bateman, M.D., Thomas, D.S.G., Singhvi, A.K., 2003. Extending the aridity record of the Southwest Kalahari: current problems and future perspectives. Quat. Int. 111, 37–49.
Bateman, M.D., Boulter, C.H., Carr, A.S., Frederick, C.D., Peter, D., Wilder, M., 2007. Preserving the palaeoenvironmental record in drylands: bioturbation and its significance for luminescence-derived chronologies. Sediment. Geol. 195, 5–19.
Birkeland, P.W., 1999. Soils and Geomorphology. Oxford University Press, New York.
Bond, G.W., Heinrich, H., Broecker, W., Labeyrie, L., McManus, J., Andrews, J., Huon, S., Jantschick, R., Clasen, S., Simet, C., Tedesco, K., Klas, M., Bonani, G., Ivy, S., 1992. Evidence for massive discharges of icebergs into the North Atlantic Ocean during the last glacial period. Nature 360, 245–249.
Burrough, S.L., Thomas, D.S.G., Singarayer, J.S., 2009. Late Quaternary hydrological dynamics in the Middle Kalahari: forcing and feedbacks. Earth-Sci. Rev. 96, 313–326.
Burrough, S.L., Thomas, D.S.G., 2013. Central southern Africa at the time of the African Humid Period: a new analysis of Holocene palaeoenvironmental and palaeoclimatic data. Quat. Sci. Rev. 80, 29–46.
Butzer, K.W., 1971. Fine alluvial fills in the Orange and Vaal basins of South Africa. Proc. Assoc. Am. Geogr. 3, 41–48.
Butzer, K.W., 1984. Late Quaternary environments in South Africa. In: Vogel, J.C. (Ed.), Late Cainozoic Palaeoclimates of the Southern Hemisphere. Balkema, Rotterdam, pp. 236–264.
Butzer, K.W., Fock, G.J., Stickenrath, R., Zilch, A., 1973. Paleohydrology of Late Pleistocene lake Alexandersfontein, Kimberley, South Africa. Nature 243, 328–330.
Chase, B.M., 2009. Evaluating the use of dune sediments as a proxy for palaeoaridity: a southern African case study. Earth-Sci. Rev. 93, 31–45.
Chase, B.M., 2010. South African palaeoenvironments during marine oxygen isotope stage 4: a context for the Howiesons Poort and Still Bay industries. J. Archaeol. Sci. 37, 1359–1366.
Chase, B.M., Meadows, M.E., 2007. Late Quaternary dynamics of southern Africa's winter rainfall zone. Earth-Sci. Rev. 84, 103–138.
Chase, B.M., Meadows, M.E., Scott, M.L., Thomas, D.S.G., Marais, E., Sealy, J., Reimer, P.J., 2009. A record of rapid Holocene climate change preserved in hyrax middens from southwestern Africa. Geology 37, 703–706.
Chiang, J.C.H., Bitz, C.M., 2005. Influence of high latitude ice cover on the marine Intertropical Convergence Zone. Clim. Dyn. 25, 477–496.
Churchill, S.E., Brink, J.S., Berger, L.R., Hutchison, R.A., Rossouw, L., Stynder, D., Hancox, P.J., Brandt, D., Woodborne, S., Lock, J.C., Scott, L., Ungar, P., 2000. Erfkroon: a new Florisian fossil locality from fluvial contexts in the western Free State, South Africa. South Afr. J. Sci. 96, 161–163.
Dearing, J.A., 1994. Environmental Magnetic Susceptibility. Chi Publishing, Kenilworth, UK.
Duller, G.A.T., 2003. Distinguishing quartz and feldspar in single grain luminescence measurements. Radiat. Meas. 37, 161–165.
Duller, G.A.T., 2004. Luminescence dating of Quaternary sediments: recent advances. J. Quat. Sci. 19, 183–192.
Duller, G.A.T., 2008. Single-grain optical dating of Quaternary sediments: why aliquot size matters in luminescence dating. Boreas 37, 589–612.
Dupont, L.M., Caley, T., Kim, J.-H., Casteneda, I., Malaizé, B., Giraudeau, J., 2011. Glacial-interglacial vegetation dynamics in south eastern Africa depend on sea surface temperature variations in the west Indian Ocean. Clim. Past 7, 1209–1224.
Ekblom, A., Stabell, B., 2008. Paleohydrology of lake Nhaucati (southern Mozambique), 400 AD to present. J. Paleolimnol. 40, 1127–1141.
Gale, S.J., Hoare, P.G., 1992. Quaternary Sediments: Petrographic Methods for the Study of Unlithified Rocks. Belhaven Press and Halsted Press, New York and Toronto.
Galbraith, R.F., Roberts, R.G., Laslett, G.M., Yoshida, H., Olley, J.M., 1999. Optical dating of single and multiple grains of quartz from Jimnium rock shelter, northern Australia: part I, experimental design and statistical models. Archaeometry 41, 339–364.
Gasse, F., Chalié, F., Vincens, A., Williams, M.A.J., Williamson, D., 2008. Climatic patterns in equatorial and southern Africa from 30,000 to 10,000 years ago reconstructed from terrestrial and near-shore proxy data. Quat. Sci. Rev. 27, 2316–2340.
Goddard, L., Graham, N.E., 1999. Importance of the Indian Ocean for simulating rainfall anomalies of eastern and southern Africa. J. Geophys. Res. 104, 19099–19116.
Goudie, A.S., 1983. Calcrete. In: Goudie, A.S., Pye, K. (Eds.), Chemical Sediments and Geomorphology. Academic Press, New York, pp. 93–131.
Guyodo, Y., LaPara, T.M., Anschutz, A.J., Penn, R.L., Banerjee, S.K., Geiss, C.F., Zanner, W., 2006. Rock magnetic, chemical and bacterial community analysis of a modern soil from Nebraska. Earth Planet. Sci. Lett. 251, 168–178.
Hao, Q., Oldfield, F., Bloemendal, J., Guo, Z., 2008. The magnetic properties of loess and palaeosol samples from the Chinese Loess Plateau spanning the last 22 million years. Palaeogeogr. Palaeoclimatol. Palaeoecol. 260, 389–404.
Hao, Q., Oldfield, F., Bloemendal, J., Torrent, J., Guo, Z., 2009. The record of changing hematite and goethite accumulation over the last 22 Ma on the Chinese Loess Plateau, from magnetic measurements and Diffuse Reflectance Spectroscopy. J. Geophys. Res. 114, B12101.
Holmes, P.J., Barker, C.H., 2006. Geological and geomorphological controls on the physical landscape of the Free State. South Afr. Geogr. J. 88, 3–10.
Holmgren, K., Lee-Thorp, J.A., Cooper, G.R.J., Lundblad, K., Partridge, T.C., Scott, L., Sithaldeen, R., Talma, A.S., Tyson, P.D., 2003. Persistent millennial-scale climatic variability over the past 25,000 years in southern Africa. Quat. Sci. Rev. 22, 2311–2326.
Jacobs, Z., Roberts, R.G., 2007. Advances in optically stimulated luminescence dating of individual grains of quartz from archaeological deposits. Evol. Anthropol. 16, 210–223.
Jacobs, Z., Roberts, R.G., Galbraith, R.F., Deacon, H.J., Grun, R., Mackay, A., Mitchell, P., Vogelsang, R., Wadley, L., 2008. Ages for the Middle Stone Age of southern Africa: implications for human behavior and dispersal. Science 322, 733–735.
Jain, M., Murray, A.S., Bøtter-Jensen, L., 2004. Optically stimulated luminescence dating: how significant is incomplete light exposure in fluvial environments. Quaternaire 15, 143–157.
Jenny, H., 1941. Factors of Soil Formation. McGraw-Hill, New York.
Ji, J.F., Balsam, W., Lu, H.Y., Sun, Y.B., Xu, H.F., 2004. High resolution hematite/goethite records from Chinese loess sequences for the last glacial-interglacial cycle: rapid climatic response of the East Asian Monsoon to the tropical Pacific. Geophys. Res. Lett. 31, L03207.
Johnson, B.J., Miller, G.H., Fogel, M.L., Beaumont, P.B., 1997. The determination of late Quaternary paleoenvironments at Equus Cave, South Africa, using stable isotopes and amino acid racemization in ostrich eggshell. Palaeogeogr. Palaeoclimatol. Palaeoecol. 136, 121–137.
Johnson, T.C., Brown, E.T., McManus, J., Barry, S., Barker, P., Gasse, F., 2002. A high-resolution palaeoclimatic record spanning the past 25,000 years in southern East Africa. Science 296, 113–132.
Jouzel, J., Masson-Delmotte, V., Cattani, O., Dreyfus, G., Falourd, S., Hoffmann, G., Minster, B., Nouet, J., Barnola, J.M., Chappellaz, J., Fischer, H., Gallet, J.C., Johnsen, S., Leuenberger, L., Loulergue, L., Luethi, D., Oerter, H., Parrenin, F., Raisbeck, G., Raynaud, D., Schilt, A., Schwander, J., Selmo, E., Souchez, R., Spanhni, R., Stauffer, B., Steffensen, J.P., Stenni, B., Stocker, T.F., Tison, J.L.,

Werner, M., Wolff, E.W., 2007. Orbital and millennial Antarctic climate variability over the past 800,000 years. Science 317, 793–797.
Jury, M.R., Enfield, D.B., Melice, M.L., 2002. Tropical monsoons around Africa: stability of El Nino-Southern Oscillation associations and links with continental climate. J. Geophys. Res. 107, 3151.
Kämpf, N., Schwertmann, U., 1983. Goethite and hematite in a climosequence in Southern Brazil and their application in classification of kaolinitic soils. Geoderma 29, 27–39.
Keen-Zebert, A., Tooth, S., Rodnight, H., Duller, G.A.T., Roberts, H.M., Grenfell, M., 2013. Late Quaternary floodplain reworking and the preservation of alluvial sedimentary archives in unconfined and confined river valleys in the eastern interior of South Africa. Geomorphology 185, 54–66.
Kruger, A.C., 2004. Climate of South Africa. Climate regions. WS 45. South African Weather Service.
Kutzbach, J.E., 1981. Monsoon climate of the early Holocene: climate experiment with the Earth's orbital parameters for 9000 years ago. Science 214, 59–61.
Lee-Thorp, J.A., Beaumont, P.B., 1995. Vegetation and seasonality shifts during the late Quaternary deduced from $^{13}C/^{12}C$ ratios of grazers at Equus Cave, South Africa. Quat. Res. 43, 426–432.
Lee-Thorp, J.A., Holmgren, K., Lauritzen, S.-E., Linge, H., Moberg, A., Partridge, T.C., Stevenson, C., Tyson, P.D., 2001. Rapid climate shifts in the southern African interior throughout the mid to late Holocene. Geophys. Res. Lett. 28, 4507–4510.
Lindquist, A.K., Feinberg, J.M., Waters, M.R., 2011. Rock magnetic properties of a soil developed on an alluvial deposit at Buttermilk Creek, Texas, USA. Geochem. Geophys. Geosys. 12, 1–11.
Liu, Q., Deng, C., Torrent, J., Zhu, R., 2007. Review of recent developments in mineral magnetism of the Chinese loess. Quat. Sci. Rev. 26, 368–385.
Liu, Q.S., Torrent, J., Barrón, V., Duan, Z.Q., Bloemendal, J., 2011. Quantification of hematite from the visible diffuse reflectance spectrum: effects of aluminium substitution and grain morphology. Clay Miner. 46, 137–147.
Liu, Q.S., Roberts, A.P., Larrasoana, J.C., Banerjee, S.K., Guyodo, Y., Tauxe, L., Oldfield, F., 2012. Environmental magnetism: principles and applications. Rev. Geophys. 50, RG4002.
Long, X., Ji, J., Balsam, W., 2011. Rainfall-dependent transformations of iron oxides in a tropical saprolite transect of Hainan Island, South China: spectral and magnetic measurements. J. Geophys. Res. 116, F03015.
Lyons, R., Oldfield, F., Williams, E., 2010. Mineral magnetic properties of surface soils and sands across four North African transects and links to climatic gradients. Geochem. Geophys. Geosys. 11, Q08023.
Lyons, R., Oldfield, F., Williams, E., 2012. The possible role of magnetic measurements in the discrimination of Sahara/Sahel dust sources. Earth Surf. Process. Landf. 37, 594–606.
Lyons, R., Tooth, S., Duller, G.A.T., 2013. Chronology and controls of gully (donga) formation in the upper Blood River catchment, KwaZulu-Natal, South Africa: evidence for a climatic driver of erosion. Holocene 23, 1875–1887.
Maher, B.A., 1998. Magnetic properties of modern soils and Quaternary loessic paleosols: paleoclimatic implications. Palaeogeogr. Palaeoclimatol. Palaeoecol. 137, 25–54.
Maher, B.A., 2011. The magnetic properties of Quaternary aeolian dusts and sediments, and their palaeoclimatic significance. Aeolian Res. 3, 87–145.
Maher, B.A., Taylor, R.M., 1988. Formation of ultrafine-grained magnetite in soils. Nature 336, 368–370.
Maher, B., Alekseev, A., Alekseev, T., 2003a. Magnetic mineralogy of soils across the Russian steppe: climatic dependence of pedogenic magnetite formation. Palaeogeogr. Palaeoclimatol. Palaeoecol. 201, 321–341.
Maher, B., MengYu, H., Roberts, H.M., Wintle, A.G., 2003b. Holocene loess accumulation and soil development at the western edge of the Chinese Loess Plateau: implications for magnetic proxies of palaeorainfall. Quat. Sci. Rev. 22, 445–451.
Maher, B.A., Thompson, R., 1995. Paleorainfall reconstructions from pedogenic magnetic susceptibility variations in the Chinese loess and paleosols. Quat. Res. 44, 383–391.
Martínez-Méndez, G., Zahn, R., Hall, I.R., Peeters, F.J.C., Pena, L.D., Cacho, I., Negre, C., 2010. Contrasting multiproxy reconstructions of surface ocean hydrography in the Agulhas Corridor and implications for the Agulhas Leakage during the last 345,000 years. Paleoceanography 25, PA4227.
Marzin, C., Braconnot, P., 2009. Variations of Indian and African monsoons induced by insolation changes at 6 and 9.5 kyr BP. Clim. Dyn. 33, 215–231.
Maslin, M.A., Christensen, B., 2007. Tectonics, orbital forcing, global climate change, and human evolution in Africa: introduction to the African paleoclimate special volume. J. Hum. Evol. 53, 443–464.
Mucina, L., Rutherford, M.C., 2006. The Vegetation of South Africa, Lesotho and Swaziland. In: Strelitzia 19. South African National Biodiversity Institute, Pretoria.
Murray, A.S., Wintle, A.G., 2000. Luminescence dating of quartz using an improved single-aliquot regenerative-dose protocol. Radiat. Meas. 32, 57–73.
Nanson, G.C., Tooth, S., 1999. Arid-zone rivers as indicators of climate change. In: Singhvi, A.K., Derbyshire, E. (Eds.), Paleoenvironmental Reconstruction in Arid Lands. Oxford and IBH, New Delhi and Calcutta, pp. 75–216.
Nicholson, S.E., Nash, D.J., Chase, B.M., Grab, S.W., Shanahan, T.M., Verschuren, D., Asrat, A., Lézine, A.-M., Umer, M., 2013. Temperature variability over Africa during the last 2000 years. Holocene 23, 1085–1094.
Norström, E., Scott, L., Partridge, T.C., Risberg, J., Holmgren, K., 2009. Reconstruction of environmental and climate changes at Braamhoek wetland, eastern escarpment South Africa, during the last 16,000 years with emphasis on the Pleistocene-Holocene transition. Palaeogeogr. Palaeoclimatol. Palaeoecol. 271, 240–258.
Oldfield, F., Yu, L., 1994. The influence of particle size variations on the magnetic properties of sediments from the north-eastern Irish Sea. Sedimentology 41, 1093–1108.
Oldfield, F., Crowther, J., 2007. Establishing fire incidence in temperate soils using magnetic measurements. Palaeogeogr. Palaeoclimatol. Palaeoecol. 249, 362–369.
Partridge, T.C., deMenocal, P.B., Lorentz, S.A., Paiker, M.J., Vogel, J.C., 1997. Orbital forcing of climate over South Africa: a 200,000-year rainfall record from the Pretoria Saltpan. Quat. Sci. Rev. 16, 1125–1133.
Peeters, F.J.C., Acheson, R., Brummer, G.-J.A., de Ruijter, W.P.M., Schneider, R.R., Ganssen, G.M., Ufkes, E., Kroon, D., 2004. Vigorous exchange between the Indian and Atlantic oceans at the end of the past five glacial periods. Nature 430, 661–665.
Petit, J.R., Jouzel, J., Raynaud, D., Brakov, N.I., Barnola, J.-M., Basile, I., Bender, M., Chappellaz, J., Davis, M., Delaygue, G., Delmotte, M., Kotlyakov, V.M., Legrand, M., Lipenkov, V.Y., Lorius, C., Pepin, L., Ritz, C., Saltzman, E., Stievenard, M., 1999. Climate and atmospheric history of the past 420,000 years from the Vostok ice core, Antarctica. Nature 399, 429–436.
Prescott, J.R., Hutton, J.T., 1994. Cosmic ray contributions to dose rates for luminescence and ESR dating: large depths and long-term time variations. Radiat. Meas. 23, 497–500.
Reid, I., 2009. River landforms and sediments: evidence of climatic change. In: Parsons, A.J., Abrahams, A.D. (Eds.), Geomorphology of Desert Environments, second ed. Springer Science, Berlin, pp. 695–721.
Rodnight, H., Duller, G.A.T., Wintle, A.G., Tooth, S., 2006. Assessing the reproducibility and accuracy of optical dating of fluvial deposits. Quat. Geochronol. 1, 109–120.
Rowan, A.V., Roberts, H.M., Jones, M.A., Duller, G.A.T., Covey-Crump, S., Brocklehurst, S.H., 2012. Optically stimulated luminescence dating of glaciofluvial sediments on the Canterbury Plains, South Island, New Zealand. Quat. Geochronol. 8, 10–22.
Schefuß, E., Kuhlmann, H., Mollenhauer, G., Prange, M., Pätzold, J., 2011. Forcing of wet phases in southeast Africa over the past 17,000 years. Nature 480, 509–512.
Scheinost, A.C., Chavernas, A., Barrón, V., Torrent, J., 1998. Use and limitations of the second-derivative diffuse reflectance spectroscopy in the visible to near-infrared range to identify and quantify Fe oxide minerals in soils. Clays Clay Miner. 46, 528–536.
Schmidt, F., Oberhänsli, H., Wilkes, H., 2014. Biocoenosis response to hydrological variability in Southern Africa during the last 84 ka BP: a study of lipid biomarkers and compound-specific stable carbon and hydrogen isotopes from the hypersaline Lake Tswaing. Glob. Planet. Change 112, 92–104.
Schwertmann, U., 1985. The effect of pedogenic environments on iron oxide minerals. Adv. Soil Sci. 1, 172–200.
Schwertmann, U., Taylor, R.M., 1989. Iron oxides. In: Dixon, J.B., Weed, S.E. (Eds.), Minerals in Soil Environments, second ed. Soil Science Society of America, Madison Wisconsin, USA, pp. 379–438.
Scott, L., Holmgren, K., Talma, A.S., Woodborne, S., Vogel, J.C., 2003. Age interpretation of the Wonderkrater spring sediments and vegetation change in the Savanna Biome, Limpopo province, South Africa. South Afr. J. Sci. 99, 484–488.
Shaw, P.A., Thomas, D.S.G., Nash, D.J., 1992. Late Quaternary fluvial activity in the dry valleys (mekgacha) of the middle and southern Kalahari, southern Africa. J. Quat. Sci. 7, 273–281.
Sonzogni, C., Bard, E., Rostek, F., 1998. Tropical sea-surface temperatures during the last glacial period: a view based on alkenones in Indian Ocean sediments. Quat. Sci. Rev. 17, 1185–1201.
Stager, J.C., Ryves, D.B., Chase, B.M., Pausata, F.S.R., 2011. Catastrophic drought in the Afro-Asian monsoon region during Heinrich event 1. Science 331, 1299–1302.
Stager, J.C., Mayewski, P.A., White, J., Chase, B.M., Neumann, F.H., Meadows, M.E., King, C.D., Dixon, D.A., 2012. Precipitation variability in the winter rainfall zone of South Africa during the last 1400 yr linked to the austral westerlies. Clim. Past 8, 877–887.
Stute, M., Talma, A.S., 1998. Glacial temperatures and moisture transport regimes reconstructed from noble gas and $\delta^{18}O$, Stampriet aquifer, Namibia. In: Isotope Techniques in the Study of Past and Current Environmental Changes in the Hydrosphere and the Atmosphere. IAEA Vienna Symposium, 1997, Vienna, pp. 307–328.
Stuut, J.B.W., Crosta, X., Van der Borg, K., Schneider, R., 2004. Relationship between Antarctic sea ice and southwest African climate during the late Quaternary. Geology 32, 909–912.
Tanner, L.H., 2010. Continental carbonates as indicators of paleoclimate. In: Alonso-Zarza, A.M., Tanner, L.H. (Eds.), Carbonates in Continental Settings: Facies, Environment, and Processes, Developments in Sedimentology, vol. 62. Elsevier, Amsterdam, pp. 179–214.
Thackeray, J.F., 1990. Temperature indices from Late Quaternary sequences in South Africa: comparisons with the Vostok core. South Afr. Geogr. J. 72, 47–49.
Tite, M.S., Linington, R.E., 1975. Effect of climate on the magnetic susceptibility of soils. Nature 265, 565–566.
Thomas, D.S.G., 2013. Reconstructing palaeoclimates and palaeoenvironments in drylands: what can landform analysis contribute? Earth Surf. Process. Landf. 38, 3–16.
Thomas, D.S.G., Burrough, S.L., 2012. Interpreting geoproxies of late Quaternary climate change in African drylands: implications for understanding environmental change and early human behaviour. Quat. Int. 253, 5–17.

Thomas, D.S.G., Burrough, S.L., 2013. Luminescence-based dune chronologies in southern Africa: analysis and interpretation of dune database records across the subcontinent. Quat. Int. (in press).
Thomas, D.S.G., Burrough, S.L., Parker, A.G., 2012. Extreme events as drivers of early human behaviour in Africa? The case for variability, not catastrophic drought. J. Quat. Sci. 27, 7–12.
Tooth, S., 2007. Arid geomorphology: investigating past, present and future changes. Prog. Phys. Geogr. 31, 319–335.
Tooth, S., 2012. Arid geomorphology: changing perspectives on timescales of change. Prog. Phys. Geogr. 36, 262–284.
Tooth, S., Brandt, D., Hancox, P.J., McCarthy, T.S., 2004. Geological controls on alluvial river behaviour: a comparative study of three rivers on the South African Highveld. J. Afr. Earth Sci. 38, 79–97.
Tooth, S., Rodnight, H., Duller, G.A.T., McCarthy, T.S., Marren, P.M., Brandt, D., 2007. Chronology and controls of avulsion along a mixed bedrock-alluvial river. Geol. Soc. Am. Bull. 119, 452–461.
Tooth, S., Hancox, P.J., Brandt, D., McCarthy, T.S., Jacobs, Z., Woodborne, S.M., 2013. Controls on the genesis, sedimentary architecture, and preservation potential of dryland alluvial successions in stable continental interiors: insights from the incising Modder River, South Africa. J. Sediment. Res. 83, 541–561.
Torrent, J., 1976. Soil development in a sequence of river terraces in northern Spain. Catena 3, 137–151.
Torrent, J., Barron, V., 2002. Diffuse reflectance spectroscopy of iron oxides. In: Hubbard, A.T. (Ed.), Encyclopedia of Surface and Colloid Science. Taylor and Francis, New York, pp. 1438–1446.
Torrent, J., Schwertmann, U., Schulze, D.G., 1980. Iron oxide mineralogy of some soils of two river terrace sequences in Spain. Geoderma 25, 191–208.
Torrent, J., Barrón, V., Liu, Q.S., 2006. Magnetic enhancement is linked to and precedes hematite formation in aerobic soil. Geophys. Res. Lett. 33, L02401.
Torrent, J., Liu, Q., Bloemendal, J., Barron, V., 2007. Magnetic enhancement and iron oxides in the upper Luochuan loess-paleosol sequence, Chinese Loess Plateau. Soil Sci. Soc. Am. J. 71, 1570–1578.
Truc, L., Chevalier, M., Favier, C., Cheddadi, R., Meadows, M.E., Scott, L., Carr, A.S., Smith, G.F., Chase, B.M., 2013. Quantification of climate change for the last 20,000 years from Wonderkrater, South Africa: implications for the long-term dynamics of the Intertropical Convergence Zone, 386, 575–587.
Tyson, P.D., Karlen, W., Holmgren, K., Heiss, G.A., 2000. The Little Ice Age and medieval warming in South Africa. South Afr. J. Sci. 96, 121–126.
Verster, E., van Rooyen, T.H., 1999. Palaeosols on a fluvial terrace at Driekop, Northern Province, South Africa as indictors of climatic changes during the late Quaternary. Quat. Int. 57–58, 229–235.
Walden, J., Oldfield, F., Smith, J. (Eds.), 1999. Environmental Magnetism: a Practical Guide. Quaternary Research Association, Technical Guide.
Watson, A., 1985. Structure, chemistry and origins of gypsum crusts in southern Tunisia and the central Namib Desert. Sedimentology 32, 855–875.
Woodborne, S., Melice, J.-L., Scholes, R.J., 2008. Long-term sunspot forcing of savanna structure inferred from carbon and oxygen isotopes. Geophys. Res. Lett. 35, L02711.
Worm, H.-U., 1998. On the superparamagnetic-stable single domain transition for magnetite, and frequency dependency of susceptibility. Geophys. J. Int. 133, 201–206.
Zhou, L.P., Oldfield, F., Wintle, A.G., Robinson, S.G., Wang, J.T., 1990. Partly pedogenic origin of magnetic variations in Chinese loess. Nature 346, 737–739.
Ziegler, M., Simon, M.H., Hall, I.R., Barker, S., Stringer, C., Zahn, R., 2013. Development of Middle Stone Age innovation linked to rapid climate change. Nat. Commun. 4, 1–9.